THE FORMATION OF EPITAXIALLY STABILIZED NICKEL AND COBALT SILICIDES BY PULSED LASER ANNEALING

by

Thulani M. Kubeka

Thesis submitted to the Faculty of Science
of the University of Cape Town in fulfilment of the requirements
for the Master of Science degree in Physics

Department of Physics
University of Cape Town

29 June 2001

Abstract

The formation of epitaxially stabilised nickel and cobalt silicides by pulsed laser annealing has been investigated. Thermally grown NiSi and CoSi on Si<111> substrate were irradiated with laser pulses in the energy density range between $0.4 - 1.0\ J/cm^2$ in an attempt to produce epitaxially stabilized silicides. The analysis was carried out using well established RBS and channelling techniques.

In the bulk form, and in thin films, NiSi has an orthorhombic MnP crystal structure and cannot grow epitaxially on the cubic silicon substrate and channelling is not observed in the silicides thus prepared. Since NiSi melts at a temperature 400°C below silicon, it is possible to melt the whole NiSi film without melting the substrate. The presence of channelling in the NiSi film observed after laser annealing at lower energy densities was an indication that complete melting of the film had occured allowing for re-ordering of atoms in the melt. At higher energy densities a significant amount of interdiffusion between the NiSi film and silicon occured. The stability of the produced metastable phase of NiSi was tested by furnace annealing. It was found that the samples readily transforms back to the orthorhombic MnP phase of the NiSi layer upon annealing at temperatures as low as 200°C for 30 minutes.

Although both silicon and CoSi are cubic in form, CoSi cannot grow epitaxially on silicon because of the large lattice mismatch $\sim 18\%$. Since CoSi has a comparable melting temperature to silicon it is not possible to melt the whole CoSi without inducing some melting on the substrate below it. The appearance of channelling after laser annealing was an indication that complete melting of the film had occured, allowing for re-ordering of atoms in the melt and subsequent epitaxial regrowth on the substrate. Channelling in the film detoriates after thermal annealing.

It is proposed that the appearance of channelling in the NiSi and CoSi film after laser annealing is due to the presence of the metastable phase with the CsCl structure in the film.

In an attempt to prevent the problem of interdiffusion between silicon from the sub-

strate and the CoSi film, a composite NiSi/CoSi film was devised. The presence of channelling in the composite film after annealing was taken as an indication that complete melting of the film had occured. Channelling in the composite film in the interface region is more uniform, and the interface between channelled and nonchannelled is much sharper. The channelling in the film improved slightly after annealing at higher energy density, but χ_{min} in the surface region remained poor.

Acknowledgements

I am indebted to the following people:

- My supervisor, Prof. Craig Comrie, from the Physics Department of the University of Cape Town (U.C.T.) without whose guidance, undivided attention and expert supervision skillls throughout the success of this work could not have been possible. I enjoyed spending those long hours with him preparing samples and doing "channelling" at the National Accelerator Centre (N.A.C.);

- The previous group heads, Prof. René Pretorius and Dr. Viktor Prozesky, for their warm welcome and for allowing me to use the facilities in the now newly named Materials Research Group (M.R.G.) at N.A.C.;

- The newly appointed group head of the M.R.G., Dr. Chris Theron, for his courtesy and assistance with computer software and experimental equipments especially when things could not get going;

- Messrs Karl Spinghorn, Neildine Stodart and Colin Doyle for their technical assistance and excellent operation of equipments at M.R.G;

- Dr. Cecil Churms, now employed by De Beers, for allowing me to use his CCMILLER software to draw crystal structures in my work;

- Messrs, Tshepo Ntsoane and Mlungisi Nkosi, both studying towards their M.Sc. (degree) with the M.R.G., for their friendship and for providing me accommodation when I was homeless. Once more, thanks for being there for me during those dark days;

- The Solid State Physics group of the University of Western Cape, for their constant support and interest in my work;

- National Research Foundation and N.A.C. for their financial assistance during the course of my study;

- Messrs Adriasen Govender, Given Mabala, Kevin Mayer, and Ms. Jaynie Padayachee, for providing assistance with LaTeX and *Scientific Workplace 3.0* software;
- My parents and family, for their belief in me and without whose support, I might not have reached this level of my studies;
- To all those I might have forgotten to mention for any form of support and camaraderie;

Contents

List of Figures

Chapter 1

Introduction

1.1 Overview

Ever since the invention of integrated circuits (in the 1956's), device dimensions have been shrinking. Initially this was driven by the desire to reduce costs and increase the speed of the devices. Cost issues have become less important over the years while increasing packing density of devices has become more important. Because of their low resistivity and high thermal stability, metal silicides have attracted wide interest in the microelectronic industry where they have been used as ohmic contacts, Schotty barrier, interconnects and gate electrodes. As a result of their application in the microelectronic industry metal silicides have been extensively studied and most of their properties are well known. One class of metal silicides which has only recently been discovered is that of epitaxially stabilized silicides [1, 2]. These metastable silicides are generally grown by molecular beam epitaxy (MBE). MBE technique is a layer by layer growth of films under ultra-high vacuum (UHV) conditions to produce silicide films which are truly single crystalline. The purpose of this investigation is to determine the feasibility of producing the metastable phases by pulsed laser annealing.

When a thin metal film reacts with silicon, various phases of silicides are possible. Fig. 1-1 and 1-2 shows the equilibrium phase diagrams for the Ni-Si and Co-Si systems. With

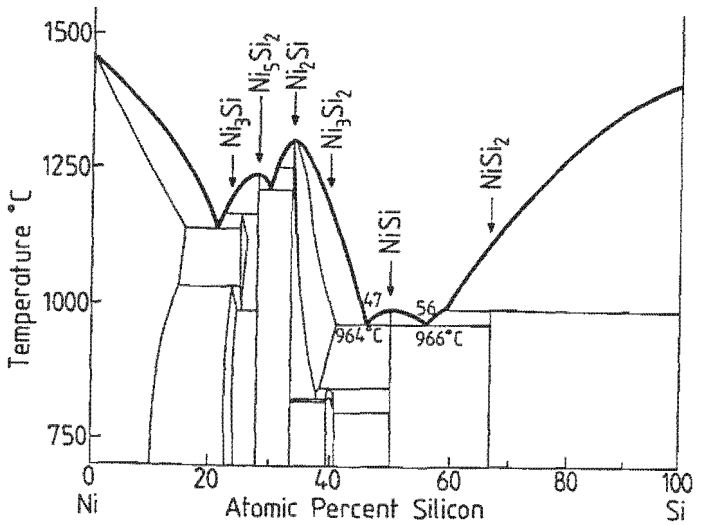

Figure 1-1: *The equilibrum phase diagram for Ni-Si system* [3].

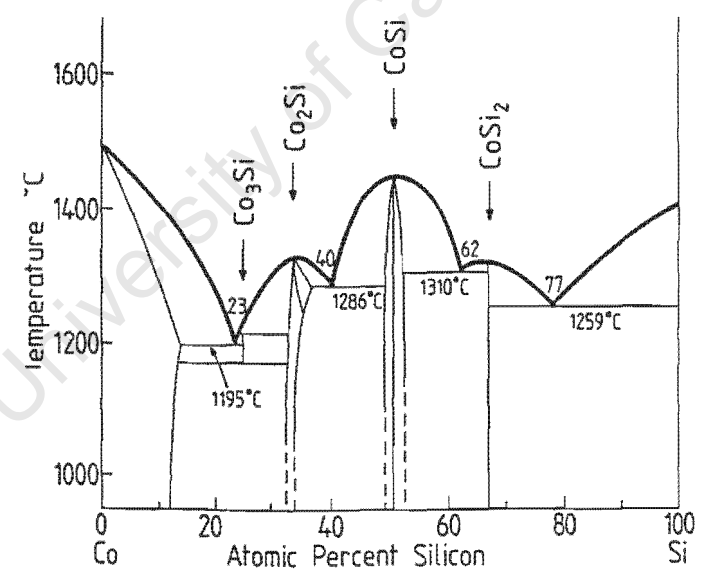

Figure 1-2: *The equilibrum phase diagram for Co-Si system* [3].

these two systems the first compound to grow is the metal rich M_2Si phase [4 – 7]. The formation temperature for Ni_2Si is as low as 200°C while that of Co_2Si is higher, around 350°C [8]. Both the Ni_2Si and Co_2Si have an orthorhombic $PbCl_2$ crystal structure and have comparable lattice parameters [9]. With excess silicon the monosilicides, NiSi and CoSi, are next to grow at temperatures around 350 and 375°C respectively[9 – 11]. NiSi has an orthorhombic MnP crystal structure while CoSi has a cubic ϵ-FeSi crystal structure [12]. The final phases to grow are disilicides, $NiSi_2$ and $CoSi_2$ [11]. $NiSi_2$ is only formed at temperature above 750°C [13] while $CoSi_2$ grows at temperature as low as 550°C [6]. Both of these compounds have cubic CaF_2 crystal structure and comparable lattice parameters [12]. Of all these silicides, $CoSi_2$ has attracted most attention because of its potential applications in the microelectronic industry. It has good thermal stability and a low resistivity of 14 $\mu\Omega$.cm.

Metal silicides growth occurs in 3 different modes of reaction, as shown in fig. 1-3, viz. diffusion, reaction and nucleation controlled. *Diffusion controlled* growth is controlled by the supply of silicon or metal to the growth interface. The diffusion path increases with growth and the growth rate is therefore proportional to (time t)$^{\frac{1}{2}}$. In our systems, Ni_2Si, Co_2Si, NiSi and CoSi growth [9, 14] are all diffusion controlled. *Reaction controlled* growth is one where growth is controlled by the rate of reaction and not the supply of Si or M to growth interface. The growth rate is therefore proportional to t (example of a reaction controlled growth is the formation of $CrSi_2$ [14]). Both diffusion and reaction controlled growth show layer-by-layer growth. Generally, with layer-by-layer growth one finds that the next phase does not begin to form until growth of the first phase has been completed. This is true for the Ni/Si system, but with cobalt one usually find that CoSi begins to grow before Co_2Si growth [9] is completed (except in the case of Co_2Si growth on amorphous silicon [15]). *Nucleation controlled* growth occurs because of a low driving force for transformation from one phase to another. Growth begins by nucleation of seeds of the new phase, followed by formation of columns extending first to the surface and thereafter spreading uniformly parallel to the substrate. Growth is therefore not

layer-by-layer and, in general, occurs very rapidly once the temperature of nucleation has been exceeded. The growth of $NiSi_2$ exhibits this non layer-by-layer growth and rough surface is indicative that its growth is nucleation controlled [16]. D'Heurle *et al.* [17] also claim that the growth of $CoSi_2$ is nucleation controlled. Even though $CoSi_2$ exhibits layer-by-layer growth, they believe that the differences in the growth of $NiSi_2$ and $CoSi_2$ results from the differences in activation energies of formation but not of their diffusion coefficients. They also claim that the kinetics of formation of $CoSi_2$ are complex because of the superposition of nucleation and diffusion effects. Nucleation ceases to be the rate controlling mechanisms in the formation of $NiSi_2$ and $CoSi_2$ when growth takes place on an amorphous silicon [15].

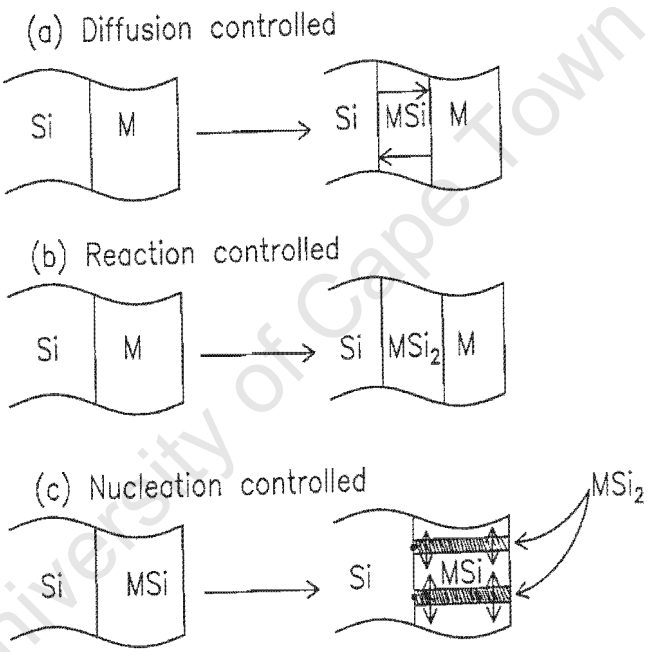

Figure 1-3: *The schematic representation of types of reactions occuring in silicon/metals, (a) diffusion controlled, (b) reaction controlled and (c) nucleation controlled reactions.*

Metal silicides are generally grown by the deposition of a metal film on a silicon substrate, followed by thermal annealing. As mentioned earlier the microelectronic industry is always on the lookout for ways of reducing the resistivity of metal silicides and

turned to epitaxial films because they have lower electrical conductivity, better thermal stability and superior interface properties than polycrystalline silicides. Epitaxial films refers to films with the same orientation as the silicon substrate, which usually requires silicides whose lattice constants are closely matched to silicon.

Silicon has a cubic (diamond) crystal structure with a lattice constant of 5.43 Å (fig. 1-4). As mentioned earlier both $CoSi_2$ and $NiSi_2$ have a cubic CaF_2 crystal structure and lattice constants of 5.41 and 5.38 Å respectively. The mismatch with silicon is $< 1.2\%$ and these disilicides can therefore be grown epitaxially on silicon. NiSi has an orthorhombic MnP crystal structure with lattice constants of 5.18, 3.34 and 5.62 Å, while CoSi has a cubic ϵ-FeSi crystal structure and a lattice constant of 4.44 Å. Because of the large lattice mismatch $> 12\%$, neither NiSi nor CoSi films can grow epitaxially on a silicon substrate [12].

1.2 Growth of epitaxial films

The first technique used to fabricate epitaxial silicides was Solid Phase Epitaxy (SPE) [14]. This entails the deposition of a pure metal layer on a silicon substrate followed by thermal annealing, resulting in the growth of the epitaxial film. Early applications of SPE, however, suffered from poor control of the processing ambients, and the quality of the epitaxial silicide was mediocre at best. Impurities incorporated during the growth and thermal annealing process can be eliminated by the use of MBE technique and this has proved to have beneficial effects on the epitaxial quality of the film [18]. As mentioned earlier MBE is a layer-by-layer growing of epitaxial films under UHV conditions to produce silicide films which are truly single crystalline.

Nowadays, high quality epitaxial films are best grown by MBE and using the "template technique" developed by Tung [19]. The template technique involves the reaction of a monolayer or submonolayer of metal with a clean semiconductor surface at room temperature. These monolayers are then annealed to produce uniform, ultra-thin, high

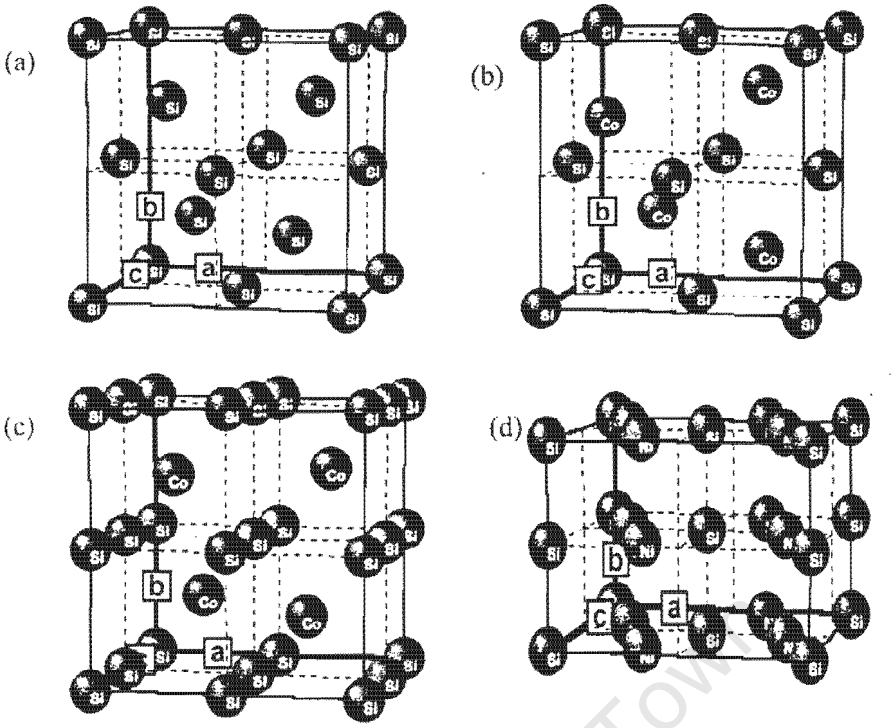

Figure 1-4: *The atomic crystal structures for (a) cubic Si(diamond) structure and a*= 5.43 Å, *(b) cubic CoSi with a =4.44* Å *and* ϵ*-FeSi structure, (c)* $CoSi_2$ *with cubic* CaF_2 *structure and a*= 5.38 Å, *(d) bulk form NiSi with an orthorhombic MnP structure and constants 5.18, 3.34 and 5.62* Å *for a, b and c respectively.*

quality, single crystalline epitaxial silicide films [20]. These ultra-thin silicide layers are then used as "templates" on which thicker epitaxial silicides can be grown at room temperature by co-evaporation of metals and silicon or just metals. The epitaxial quality of films produced by this technique is better than those produced by either SPE or conventional MBE for layers of the same thickness [19].

The first silicide reported to have been grown epitaxially on silicon was PtSi [21] in 1967. This was surprising in view of large mismatch (12%) between PtSi and silicon and then different crystal structures. PtSi has an orthorhombic MnP crystal structure with lattice constants 5.60, 5.93 and 3.60 Å, while Si is cubic (diamond) with a lattice constant of 5.43 Å. PtSi can only grow epitaxially on Si<111> but, it was not possible to

grow thick films of good epitaxial quality because of the large mismatch. Other silicides reported to have been grown epitaxially are $FeSi_2$, $TiSi_2$, $NiSi_2$, $CoSi_2$, Pd_2Si, YSi_2, and $ErSi_{2-x}$ for $(0 < x < 0.5)$ with $NiSi_2$ and $CoSi_2$ receiving the most attention.

SPE is simple, but contaminants on the substrate can inhibit the desired epitaxial quality of the film, while in MBE contaminants can be eliminated but it is a complicated process. In contrast to the above techniques, good quality epitaxial silicide layers can be produced by pulsed laser irradiation, a relatively simple technique. During laser annealing contaminants are mixed in the whole molten layer, thereby reducing their concentration [22]. Poate *et al.* [23] were the first to report the growth of silicide layers by pulsed laser irradiation of Ni, Pd or Pt films on silicon. These silicide layers were not of uniform composition but consisted of cells of Si surrounded by walls of silicides [24]. It was argued that the formation of the cellular structures was a result of the rapid quenching which lead to interfacial instabilities during recrystallization.

Tung *et al.* [25] demonstrated that the problem of single phase silicide can be overcome by using a correct starting composition. This was achieved by first furnace annealing to form an equilibrium silicide, before subjecting it to laser annealing. The growth was carried out by e-beam deposition of 300 Å of nickel on a Si<111> substrate under conventional vacuum conditions. This was followed by thermal annealing at a temperature of 800°C for 30 minutes resulting in the growth of a 1090-Å thick film of $NiSi_2$ on the substrate. The $NiSi_2$ film prepared in this manner consists of grains of normal orientation (type A), and grains rotated 180° about the normal (type B) [19, 20]. Laser irradiation of these silicides resulted in the growth of single crystalline material of type B. They also observed that a better quality of epitaxial film can be produced by performing laser irradiation on a NiSi film followed by a furnace anneal at 800°C for 30 min. The $NiSi_2$/ Si interface produced in this manner is more uniform than that grown by normal MBE or SPE techniques. The channelling yield $(\chi_{min}) \sim 3\%$ along the (111) plane showed that the crystalline quality was nearly perfect. They used the same method to grow $CoSi_2$ of good epitaxial quality on Si<111>, however, they were unable

to grow $CoSi_2$ of good epitaxial quality on Si<100> substrate.

1.3 Metastable silicides

Recently considerable interest was generated by the discovery of an epitaxially stabilized crystal structure which did not exist in the bulk form [1, 2]. Von Känel *et al.* [26] in 1992 discovered a metastable phase of FeSi which crystallizes with a CsCl crystal structure. The CsCl structure is cubic with equal number of atoms in each cell (fig. 1-5) and with a lattice constant approximately $\frac{1}{2}$ that of silicon (2.7 Å). Epitaxially stabilized [CsCl]FeSi was grown on a clean (111) Si (7×7) reconstructed substrate by depositing 2 monolayers of pure Fe at temperatures less than $< 100°C$. This was followed by co-deposition of Fe and Si at room temperature in a stoichiometric ratio 1:1 until the desired thickness between $(5 - 80$ Å) was reached. The orientation of the epitaxial stabilized FeSi films was found to be of type B.

Since both bulk Co and Fe monosilicides have the same crystal structure (ϵ-FeSi) and comparable lattice parameters [27], von Känel was lead to suspect that it might also be possible for CoSi to crystallize in the CsCl structure. Further support for this idea was that the only monosilicides to have been reported to (sometimes) crystallize with the CsCl structure are those of Ru and Rh [28] which are the $4d$ elements situated immediately below Fe and Co in the periodic table.

The epitaxially stabilized CoSi with the CsCl phase was produced by von Känel *et al.* [29] in 1995. This epitaxially stabilized CoSi was grown in two ways. (1) A thin $(3-10$ Å) template of epitaxial $CoSi_2$ was grown by stoichiometric co-deposition of Co and Si onto a (7×7) reconstructed substrate kept at room temperature, and subsequently annealed to $\sim 350°C$. Epitaxial CoSi could then be grown by MBE (co-deposition) onto this template up to a thickness of ~ 100Å at room temperature. (2) Alternatively one or two monolayers of pure Co were first deposited, followed by MBE (co-deposition) growth of CoSi also at room temperature. They reported that both methods yielded essentially the

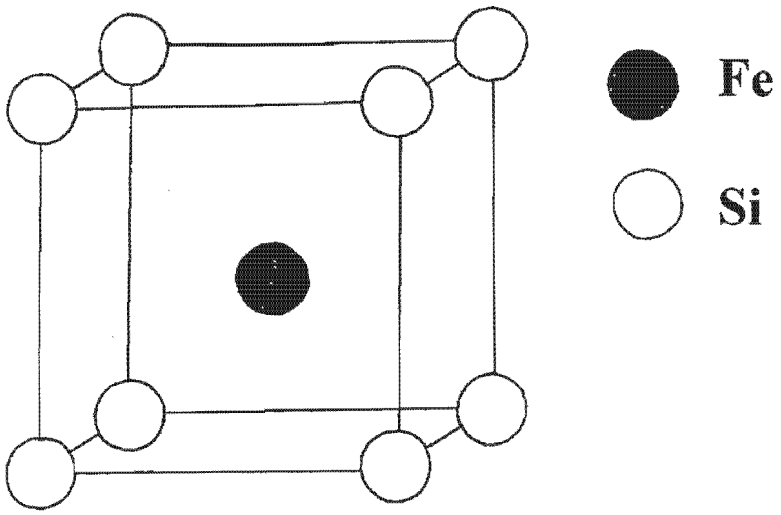

Figure 1-5: *CsCl crystal structure of FeSi, each cell contains one atom of iron and silicon.*

same results, except that the former resulted in a silicide of slightly improved crystalline quality. X-ray diffraction and transmission electron microscopy measurement confirmed that the CoSi film indeed had a CsCl phase.

Since the discovery of the CsCl phase of CoSi, attention has also been devoted to the study of $FeSi_{1+x}$ and $CoSi_{1+x}$ $(0 < x < 1)$ [29, 30] metastable phases. Pirri *et al.* [30] and Hong *et al.* [31] have found that epitaxial $CoSi_{1+x}$ silicides with $(0 < x < 1)$ could be grown on Si(111). Their studies showed that these silicides have crystal structures similar to [CsCl]FeSi silicide type grown on Si<111>. The thermal stability of the grown $CoSi_{1+x}$ film strongly depends on the concentration of Si. The $CoSi_{1+x}$ becomes more stable with x close to 1, and transforms into the more stable CaF_2 phase upon annealing at $\sim 450^{o}$C, while that with composition closer to CoSi undergoes a phase transition to the stable ϵ-FeSi form below 200°C. For x values in between, these metastable phases convert into a mixture of stable CaF_2 type $CoSi_2$ and ϵ-FeSi phases.

These non-stoichiometric compounds are of particular interest because most silicides are line compounds and cannot exist at composition which differs substantially from their stoichiometric composition. The reason why the phase can exist over a wide a range

of composition may be that the CaF_2 structure may be derived from the CsCl structure by removing $\frac{1}{2}$ of the cobalt atoms in an ordered manner. In fact the metastable $CoSi_2$ ($Co_{0.5}Si$) phase adopts a defect CsCl crystal structure with 50% vacancies distributed in a random order [30]. They observed that the metastable $Co_{0.5}Si$ phase invariably converts into stable $[CaF_2]CoSi_2$ upon annealing.

Metastable phases have also been grown by pulsed laser annealing. On irradiation the film melts and a considerable degree of undercooling in the melt is associated with the fast solidification. An undercooled melt is in a high free energy state, and it is therefore possible for it to solidify in a metastable phase. The first evidence of the formation of metastable phases after laser irradiation was noted by Tung *et al.* [25]. Laser melting and solidification of NiSi films on a Si<111> resulted in a film of composition close to $NiSi_{1.6}$ which exhibited channelling with $\chi_{min} \sim 40\%$. After thermal annealing at 800°C for 30 minutes a perfect epitaxial $NiSi_2$ film ($\chi_{min} \sim 3\%$) of type B was obtained.

A more thorough investigation into metastable phase formation by laser annealing was carried out by Baeri *et al.* [22] who showed that pulsed laser melting of a NiSi film on a Si(111) substrate can lead to the growth of a novel metastable NiSi phase exhibiting three-fold symmetry about the [111] direction. Thin 750-Å Ni films were deposited on a Si<111> substrate by electron-beam evaporation and thermally annealed for one hour at 400°C to produce a polycrystalline NiSi layers about 1700 Å in thickness. The samples thus prepared were then irradiated with a single pulse from a 35-ns Nd glass laser in the energy density range (0.3 – 2.0 J/cm^2). A quartz beam homogenizer was used to improve the lateral uniformity of the beam over a circular area 3.5 mm in diameter. After annealing at energy density of 0.7 J/cm^2 a reduction in the minimum yield at the interfacial region indicated that re-ordering of atoms in the NiSi layer had occurred at the NiSi/Si interface. By increasing the energy density the silicide layer becomes more and more epitaxially aligned with the silicon substrate. The epitaxial regrowth of the whole NiSi layer, still without a change in composition, was reported for samples laser annealed at 0.85 J/cm^2 [22]. The stoichiometry of the silicide layer remained unchanged up to an

energy density of 0.9 J/cm^2 with the best observed $\chi_{min} \sim 30\%$. At energy densities above 0.9 J/cm^2, the stoichiometry of the silicide layer changed with an average composition of $NiSi_{1.7}$ being obtained after annealing 2.0 J/cm^2. The stability of the metastable NiSi phase was tested by furnace annealing. After thermal annealing at 250°C, channelling in the silicide layer completely disappeared indicating that transformation of the metastable NiSi layer back to the MnP phase had occurred.

1.4 Scope of the present investigation

The aim of this investigation is to produce epitaxially stabilized Ni and Co silicides on a Si<111> by pulsed laser annealing. As discussed above, the formation of metastable NiSi by pulsed laser annealing has already been investigated by Baeri[22]. However, this was a time when there was not a proper understanding of metastable phases and therefore is of interest to re examine the subject in the light of the new undestanding of metastable phases. The feasibility of forming metastable phases of cobalt silicide by pulsed laser annealing has not yet been demonstrated and deserves investigation. Since NiSi melts at a temperature 400°C below silicon, it is possible to melt the whole NiSi film without melting the substrate. However with CoSi's 50°C higher melting temperature than silicon it is not possible to melt the whole CoSi without inducing some melting on the substrate below it. Non-stoichiometric $CoSi_{1+x}$ is obtained after laser annealing from the reaction of CoSi layer and silicon from the substrate. The stability of these epitaxially stabilized silicides will be tested by thermal annealing.

Chapter 2

Experimental procedure and analysis

Polished Si<111> wafers with an off-cut of $< 0.5^{o}$ were used throughout this investigation. The samples were prepared by electron beam evaporation followed by thermal annealing under vacuum conditions. Sample analysis consisted mainly of Rutherford Backscattering Spectroscopy (RBS) and channelling. The experimental procedure followed during the preparation of the samples, and the characterization used in the analysis, is described below.

2.1 Sample preparation

2.1.1 Cleaning

The Si wafers were scribed into squares of 9 mm a side, cleaned organically in an ultrasonic bath in acetone and ethanol for 5 minutes, and subsequently rinsed in de-ionized water. The wafers were then etched with a 5 % HF solution for 30 seconds to remove any native oxide layer and were then blown dry with nitrogen before being loaded into the e-beam system.

2.1.2 Vacuum deposition

The wafers were mounted onto sample holders and placed on a carousel in the e-beam system (as shown in fig. 2-1). The e-beam vacuum system consisted of a bell-jar, which enclosed a quartz crystal monitor, shutter, carousel and electron-gun. The quartz crystal monitor was used to monitor the thickness of the film during deposition. The electron gun had 3 crucibles which allowed up to 3 different materials to be evaporated onto the wafers. The baffle valve situated below the electron gun enabled the lower section to be isolated from the upper. The lower section contained an ion pump, Ti-sublimation pump and liquid nitrogen reservoir. This section was kept under vacuum, with the ion pump running, as far as possible.

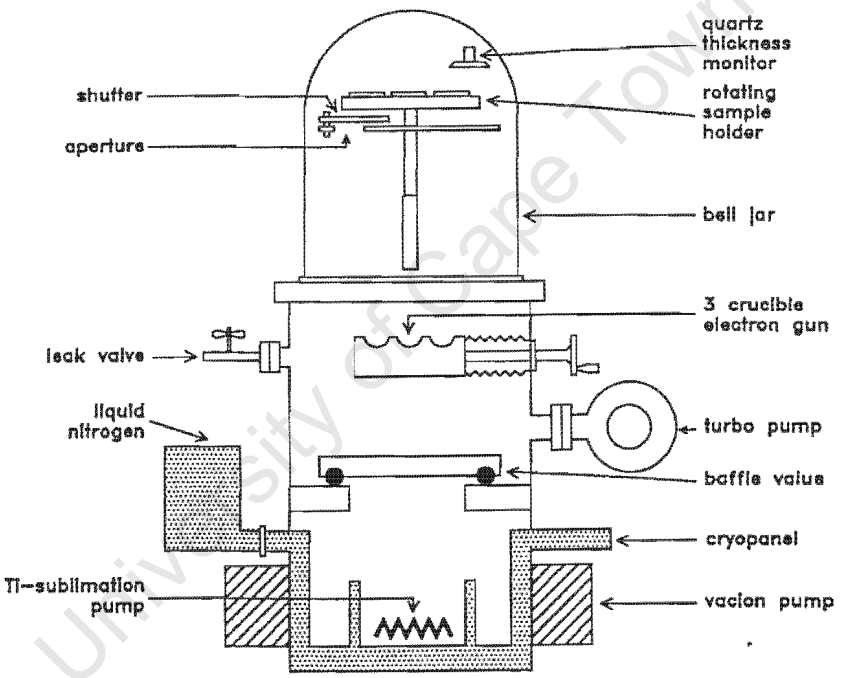

Figure 2-1: *The electron beam system used for ultra-high vacuum deposition. The baffle valve separates the system into two parts with the quartz crystal monitor attached to the growth chamber.*

On closing the bell-jar various pumps were activated sequentially. The roughing pump was used first to a create rough vacuum in the chamber and to provide the backing

pressure for the turbo molecular pump. To prevent oil diffusing back into the chamber the turbo-molecular pump was activated shortly after the roughing pump was switched on. Once the pressure had dropped below 10^{-5} Torr the baffle valve was opened up to engage the ion pump. On reaching 10^{-6} Torr the cryopanel at the base of the e-beam system was filled with liquid nitrogen to condense water vapour and other gases. The Ti-sublimation pump was used during deposition. Nickel, cobalt and Ni/Co composite films ranging in thickness from $500 - 700$ Å were deposited at a rate of about 3 Å/s onto the Si wafers at a base pressure in the low 10^{-7} Torr. After evaporation samples were left in the chamber under vacuum for a short while before being removed.

2.1.3 Furnace annealing

On removing from the e-beam system, the samples were cleaved and immediately loaded in the vacuum furnace to limit any oxidation of the film. The vacuum furnace system was pumped by a turbo-molecular pump. Once the pressure had dropped to 10^{-6} Torr the liquid nitrogen reservoir in the system was filled to condense any water vapour in the system. Thermal annealing was carried out under a base pressure of 10^{-7} Torr. These generally consisted of a 30 minute anneal at temperatures ranging from $400 - 450$°C. Under such conditions the films were transformed into monosilicides NiSi, CoSi and NiSi/CoSi films. Some of the samples were then analyzed by RBS to ensure that the films transformation was complete before being subjected to laser anneals.

2.2 Laser annealing

The laser annealing of silicides was performed under atmospheric condition using an Excimer laser of wavelength 308 nm and pulse width 30 ns. Excimer describes a class of laser systems having a gaseous mixture as active medium, excited by electrical discharges which can be tuned to give variable energies. Fig. 2-2 shows the energy curve for a diatomic molecule (A_2) in the ground and excited states [32, 33]. As shown in the plot

the ground state is repulsive and the molecule only exists in the excited state. The excited molecule A_2 is called an excimer, from the contraction of words excited dimer.

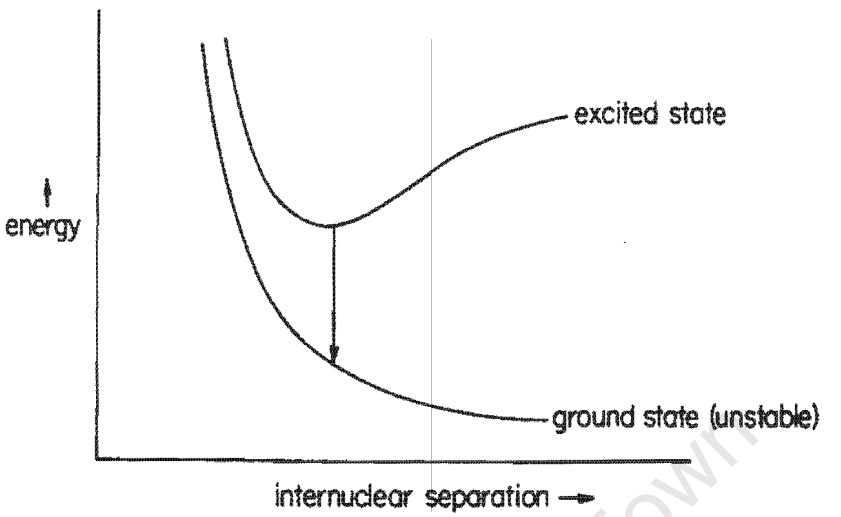

Figure 2-2: *Schematic representation of energy states of an excimer laser, the ground state does not exist because the potential energy has no local minimum.*

Emission of the laser pulse occurs on the transition between the upper bound state and the lower free state. These types of lasers have two unusual but important properties, both due to the fact that the ground state is repulsive

- Once the molecule, after undergoing the laser transition, reaches the ground state, it immediately dissociates meaning that the lower level of laser would always be empty.
- No well-defined rotational-rotational transition exists, and the transition is relatively broad-band [34].

The rare gas halides are the most efficient, emitting powerful ultraviolet (UV) radiation. The rare gas atom (Xe) is combined in the excited state, with a halogen atom

(Cl) to form an efficient rare gas halide (XeCl) excimer which on de-excitation emits a photon as shown in eq (2.1).

$$XeCl \rightarrow Xe + Cl + h\nu(308nm) \tag{2.1}$$

The use of lasers for annealing in the field of materials research was first demonstrated [35] by laser radiation of an ion-implanted material to remove damage caused by the ion implantation process. Since then lasers have found many applications in semiconductors, some of which are [36]

- formation of silicides from the deposited thin metal film on a Si substrate.
- growth of crystalline diamond from amorphous carbon films.
- formation of Al-Si contacts on shallow junctions
- laser induced diffusion and incorporation of dopants in silicon at concentrations far exceeding the solid solubility limit.

Even though the scope is wider than outlined above, all of the above processes have been collectively referred to as "laser annealing".

2.2.1 Melting, Recrystallization and Undercooling

The experimental configuration used during laser annealing is shown in fig. 2-3. Two lenses, a cylindrical and spherical were used to focus the beam and to produce a laser spot which was rectangular ($3mm \times 2mm$). The silicides were annealed with laser pulses using an energy density in the range ($0.4 - 1.0\ J/cm^2$). With the pulse width of 30 ns the power of the pulse is of the order of MW, and as all the energy is deposited in the near surface region, surface melting can be induced.

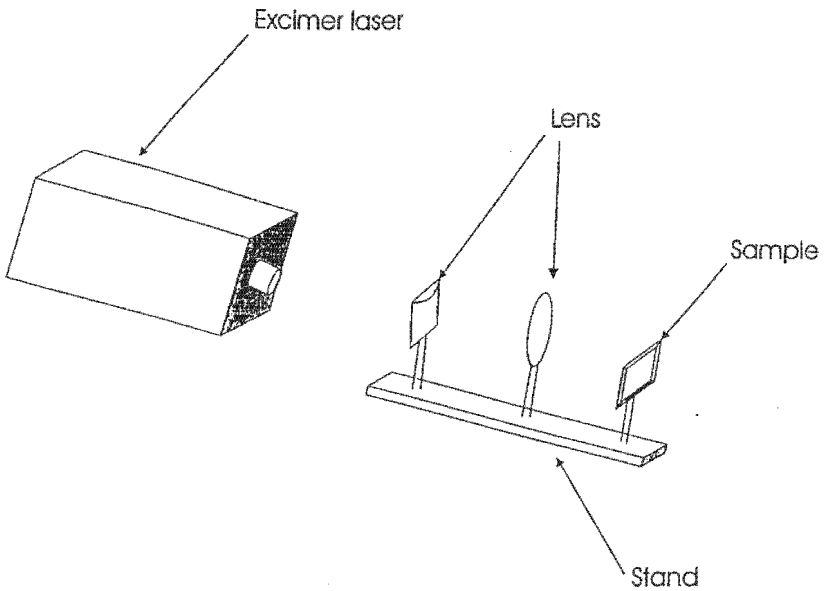

Figure 2-3: *The schematic representation of laser annealing equipment. The two lenses are placed on the path of the laser pulse to confine the beam to a square/rectangular shape.*

Heat will begin to flow from the melt into the crystalline region in the sample causing the solid-liquid interface to move deeper into the sample (as shown in fig. 2-4). The maximum melt depth depends on the energy density of the incident laser radiation. Once the melt cools down below the melting point, rapid recrystallization will occur, with the solid-liquid interface moving back to the surface of the sample. Since the whole process takes place over a time interval of the order of 100 ns, the melting and recrystallization are highly non-equilibrium processes. This means that phases which are not possible under normal thermodynamic conditions can be produced.

The phase diagrams for the Ni-Si and Co-Si system were presented earlier (in fig. 1-1 and 1-2). It is clear from the Ni-Si phase diagram that NiSi melts at a temperature $\sim$ 400K lower than Si. This means that, in principle, it is possible to melt the whole silicide layer without inducing melting of silicon in the substrate underneath it. In the case of the Co-Si system (as shown in fig. 1-2) one finds that CoSi melts at a temperature about 50°C above Si, therefore, by the time the CoSi layer has been completely melted,

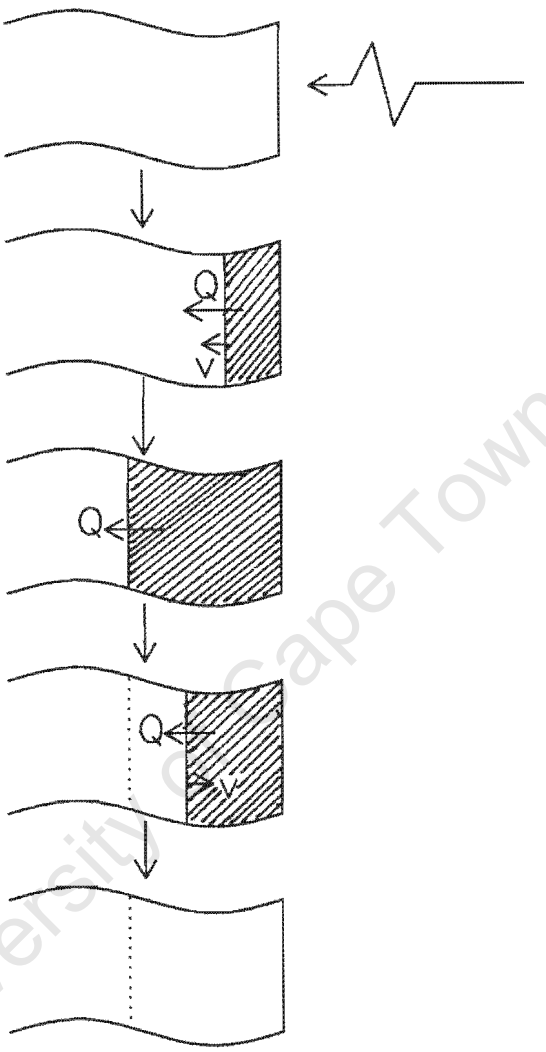

Figure 2-4: *Schematic representation showing the movement of the solid-liquid interface during melting and recrystallization. In the above figure Q is the heat flowing out of the melt and v is the direction of velocity of liquid-solid interface.*

some melting of the underlying Si will also have occurred. Since diffusion in the melt is very rapid the consequence of having molten silicon alongside the molten CoSi layer is significant interdiffusion between the two. This will result in silicon enrichment of CoSi in the region to the Si/CoSi interface.

The NiSi/CoSi films on Si (as shown in fig. 2-5) were devised to overcome the problem of interdiffusion in the CoSi-Si system[17, 37, 38]. Initially, films of nickel and cobalt were deposited on the silicon substrate. The first compounds to form in the Co-Ni-Si system are Ni_2Si and Co_2Si which are both intermixed since they both have the same crystal structure. Because of diffusion these compounds separates on forming the monosilicides with NiSi located below CoSi. It was hoped that by choosing the correct energy density, it might be possible to melt the CoSi and NiSi without melting the underlying silicon.

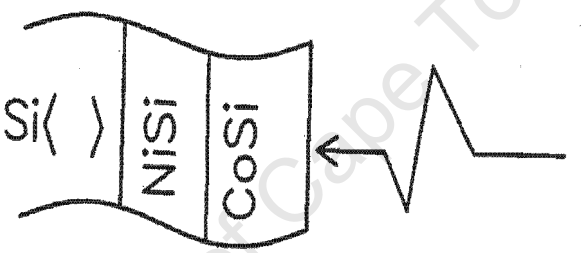

Figure 2-5: *Schematic representation of the composite NiSi/CoSi film on the silicon substrate.*

2.3 Laser calibration

Fig. 2-6 shows a linear calibration curve for the laser pulses used to anneal the samples. The energy density of the laser pulse was calibrated in order to present the energy in terms of (J/cm^2) The detector gives the signal of the laser pulse on the oscilloscope in millivolts (mV). Since it was not possible to measure the energies of the laser pulses

without removing the sample holder (see fig. 2-3), the detector was placed after the cylindrical lens in order not to tamper with the set-up. After annealing of the samples was complete, the energies of the laser pulse were measured after both lenses using measurements of the first calibration. These measured energies were multiplied by a conversion factor of 0.455 obtained from the oscilloscope to get the energy in millijoules (mJ). The energy density of the laser pulse was obtained by dividing by the energy (mJ) of the measured pulse after both lenses (spherical and concave) by the area of spot as shown by

$$E_h(mJ/cm^2) = \frac{0.455 \times mV}{area(cm^2)}. \tag{2.2}$$

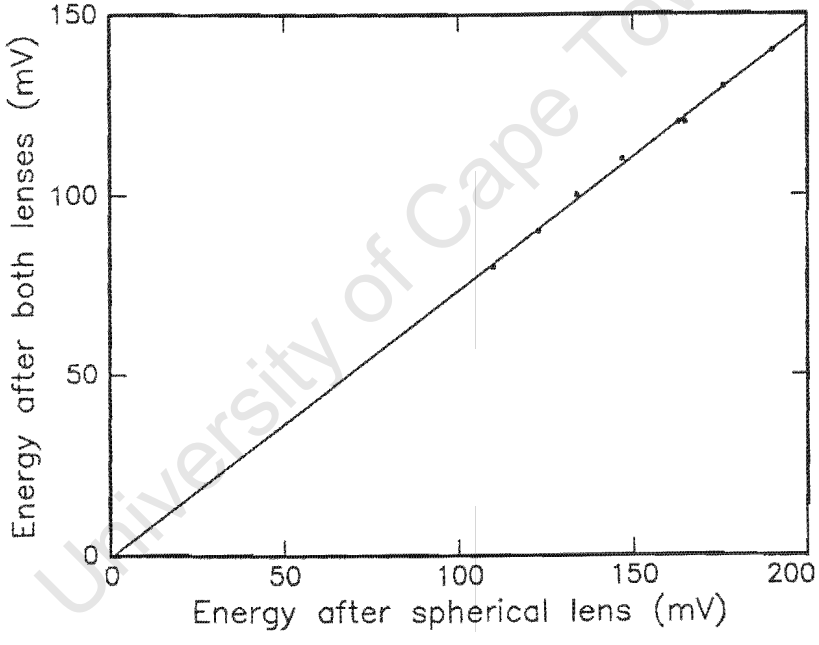

Figure 2-6: *The energy calibration curve taken after the lenses (spherical and concave) using Excimer laser.*

2.4 Rutherford Backscattering Spectroscopy (RBS)

The effect of laser annealing on the silicides was analyzed using RBS, a well established and powerful technique which is ideally suited for the analysis of thin films and layered structures. The technique dates back to 1967 when it was first used to analyze the composition of the lunar soil [39]. It has subsequently found many applications in fields both inside and outside physics. It involves the scattering of energetic $\alpha-$particle produced by an ion source (in our case the energy is raised to 2 MeV by a Van de Graaff accelerator) from the surface region of materials and deducing the mass of the atom from which the scattering took place by measuring the energy lost on scattering. The beamline and the scattering chamber were evacuated to a pressure better than 10^{-4} Torr before the $\alpha-$particles were introduced into the chamber. Two apertures, placed 3.5 m apart, were used to collimate the beam size to 1 mm in diameter and to limit divergence of the beam. During RBS [39, 40], samples were tilted 10^{o} from the normal to avoid channelling. Throughout this investigation the configuration used was one where the solid-state detector was placed to accept $\alpha-$particles backscattered through $\theta = 165^{o}$ as shown in fig (2-7).

The particle, on entering the detector, causes ionization which is then converted into an electrical signal. The signal is then passed through the preamplifier, amplifier and multichannel analyzer before being viewed on the monitor. The concepts underlying RBS analysis of thin films are discussed below.

2.4.1 Kinematic factor (k)

In Rutherford backscattering a monoenergetic α-particle of energy E_0 collides elastically with a stationary target atom and is backscattered with energy E_1 into the detector. During the collision, energy from the projectile particle is transferred to the stationary target atom, with the reduction in energy of the backscattered particle depending on the masses of the projectile and target atoms. The interaction between the projectile and

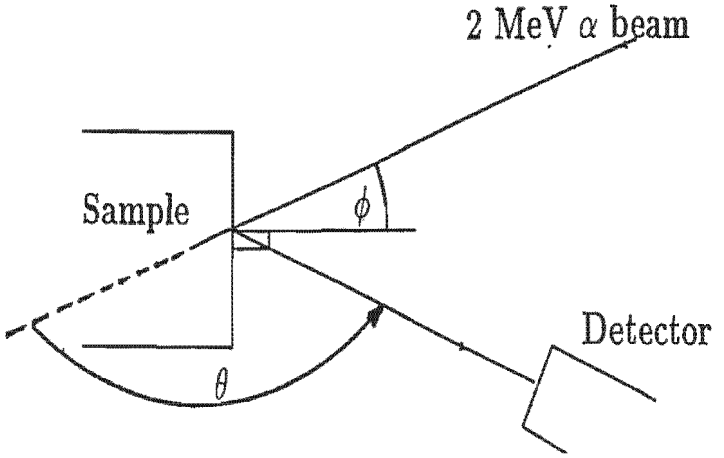

Figure 2-7: *The schematic layout for the Rutherford Backscattering experimental set-up. A collimated beam of 2 MeV α - particles is incident on the sample and is backscattered to the detector at angle $\theta = 165^0$.*

target atoms can be assumed to be elastic provided that the energy of the projectile E_0 is much greater than the binding energy of the target atom and that no resonances or nuclear reactions occur. The kinematic factor k, defined as the ratio of the projectile energy E_1 after collision to that before collision E_0 $\left(k = \frac{E_1}{E_0}\right)$, can be derived by applying the conservation of energy and momentum to the situation shown in fig. 2-8. If a projectile atom of mass m, moving at speed v_0 and energy E_0, collides with a stationary atom of mass M initially at rest, then the kinematic factor is given by

$$k = \frac{E_1}{E_0} = \left[\frac{\left(M^2 - m^2 \sin^2\theta\right)^{\frac{1}{2}} + m\cos\theta}{M+m}\right]^2 . \tag{2.3}$$

It is evident from the above equation that the kinematic factor is a function of the projectile mass m, the target mass M and the scattering angle θ. The backscattered energy E_1 depends strongly on the angle of scattering θ and attains a minimum value when the angle is 180°. It is also clear from the relationship that the energy of particles scattered by heavier elements is greater than that of those scattered by light ones. This mass dependence is used to determine the mass of the atom from which scattering took

place, which in turn provides information about the components of the material under investigation.

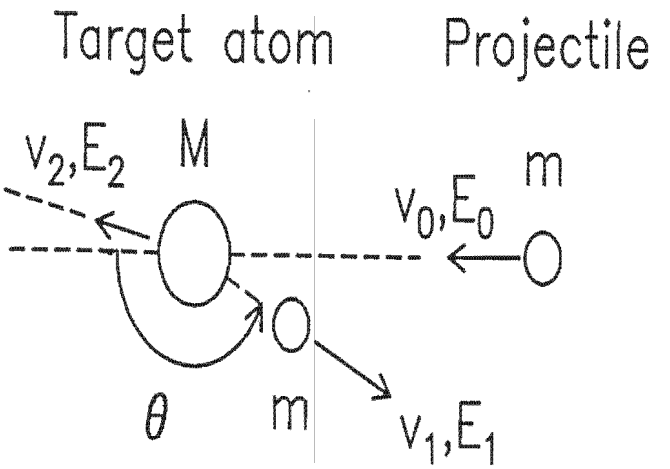

Figure 2-8: *Schematic representation of the elastic collision of the incident projectile particle of energy E_0, mass m and velocity v_0 colliding with the target of mass M initially at rest.*

2.4.2 Differential scattering cross-section $\left(\frac{d\sigma}{d\Omega}\right)$

The probability of scattering into solid angle is defined by the differential scattering cross-section

$$\frac{d\sigma}{d\Omega} = \left(\frac{zZe^2}{4E}\right)^2 \frac{4}{\sin^4\theta} \frac{\left\{\left[1-\left(\frac{m}{M}\sin\theta\right)^2\right]^{\frac{1}{2}} + \cos\theta\right\}^2}{\left[1-\left(\frac{m}{M}\sin\theta\right)^2\right]^{\frac{1}{2}}}, \tag{2.4}$$

where z and Z are the atomic numbers of the projectile and target atoms respectively. The differential scattering cross-section depends directly on the square of the atomic number of the target atom and inversely on the square of the energy of the projectile atom before scattering $\left(\frac{Z^2}{E^2}\right)$. Therefore the differential scattering cross-section will be large for high Z value and small for low value of Z and will increase as E decreases.

2.4.3 Energy loss ($\frac{dE}{dx}$)

During backscattering not all $\alpha-$particles are scattered at the surface, most scatter from atoms deeper into the sample. The energy loss may be thought of as the energy that the projectile particle expends as a result of ionization and excitation of the surrounding atoms as it travels through the sample. Consider the situation where a projectile particle scatters from two identical atoms, one at the surface and one at depth x (as shown in Fig. 2-9). The projectile particle which scatters from the target atom a distance x below the surface will have lost energy along the inward path (distance $x/\cos\theta_1$) due to energy loss, thereby resulting in a lower energy of the particle before scatter E. On scattering its energy is further reduced to kE. It then loses more energy on the outward path (distance $x/\cos\theta_2$), and finally emerges with energy E_1. The energy difference between scattering from a surface atom and one at depth x, $\Delta E = kE_0 - E_1$, can be expressed as

$$\Delta E = \left[\frac{k}{\cos\theta_1}\left(\frac{dE}{dx}\right)_{\overline{E}_{in}} + \frac{1}{\cos\theta_2}\left(\frac{dE}{dx}\right)_{\overline{E}_{out}}\right]x, \tag{2.5}$$

where $\left(\frac{dE}{dx}\right)_{\overline{E}_{in}}$ and $\left(\frac{dE}{dx}\right)_{\overline{E}_{out}}$ are the average energy losses along the inward and outward path respectively. The energy loss provides information about the depth at which scattering took place and can therefore be used to determine composition as a function of depth.

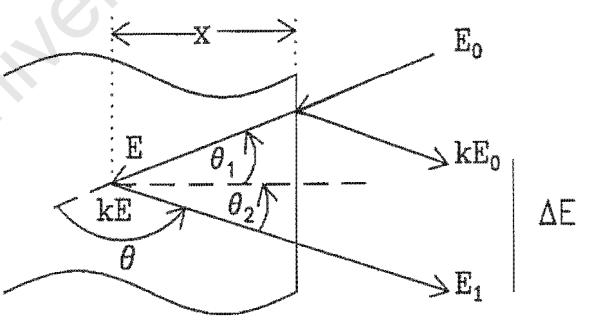

Figure 2-9: *Geometrical illustration of scattering of the incident particles on the surface and at a depth x below the surface.*

2.5 Channelling

Channelling is similar to RBS except that in RBS the direction of the incident particle is in a random crystal direction, while in channelling the direction of incident particle is aligned along one of the sample's major crystalline directions. Channelling effects arise when the incident beam is aligned along a major axis or plane of atoms which can then "steer" the energetic ions by means of gentle, small-angle collision [39, 41]. The influence of the crystal lattice on the trajectories of ions penetrating into the crystal is referred to as channelling.

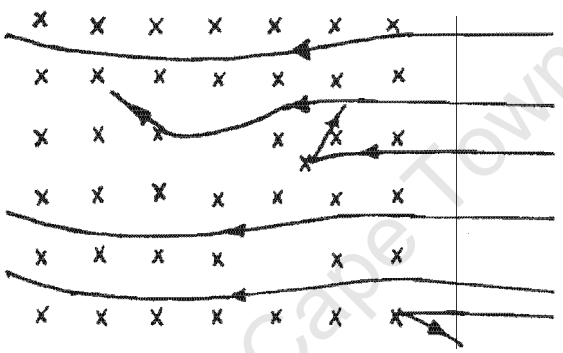

Figure 2-10: *Schematic representation of particles in an aligned beam interacting with displaced atoms to cause either backscattering events or forward scattering at angles outside the critical angle (dechannelling)*

In the case of an imperfect crystal, the channelled particle can interact with a displaced interstitial atom or vacancy in both wide-angle collisions and forward elastic scattering events as shown in fig. 2-10. The wide-angle, close encounter collisions are those leading to the direct detection of the displaced atoms through backscattering analysis. The small angle, forward scattering collisions can cause the channelled particles to be scattered at angles greater than the critical angle for channelling. This process is called dechannelling. The dechannelled particle then interacts with the nondisplaced host lattice atoms and gives rise to a higher backscattering yield than that in the case of a perfect

crystal. The backscattering yield can therefore be used to measure imperfection of the crystal lattice. Channelling can be used as an ideal non-destructive tool for a variety of applications such as:

- determination of the crystalline quality of the sample,
- determination of the depth distribution of lattice disorder in a sample,
- measuring the composition and thickness of an amorphous surface layer,
- location of impurity atoms in the lattice sites.

For channelling the sample was placed on a 3-axis goniometer (shown in fig. 2-11), allowing the sample to be tilted through $\pm$ 30° in the vertical direction (x-axis), tilted up to 180° in the horizontal direction (y-axis), or rotated through 360° about an axis along the incident beam (z-axis). To find the channelling position the sample was swept through $\pm$ 3° along x and y-axis of the sample. The sample was then aligned by measuring the backscattering yield during the sweep and fixing its orientation on the minimum in the backscattering yield.

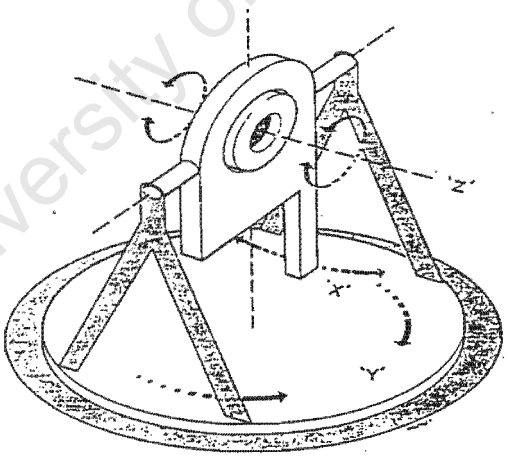

Figure 2-11: *A schematic illustration of the goniometer showing the three axis of rotation of the sample in the scattering chamber.*

2.5.1 Minimum yield ($\chi_{\min}$)

The minimum yield $\chi_{\min}$ is the ratio between the height of the aligned spectrum, (H_A), and the height of random spectrum, (H) (as shown in fig. 2-12). In the present investigation the random spectra was collected by setting the y-axis 7° off the channelling direction. By comparing the yield from aligned and random spectra (see fig. 2-12), the $\chi_{\min}$ can be obtained and is given by

$$\chi_{\min} = \frac{H_A}{H}. \tag{2.6}$$

The minimum yield $(\chi_{\min})$ for an amorphous sample would be unity, while that for an essentially perfect silicon crystalline material $\sim 2-3\%$ at room temperature.

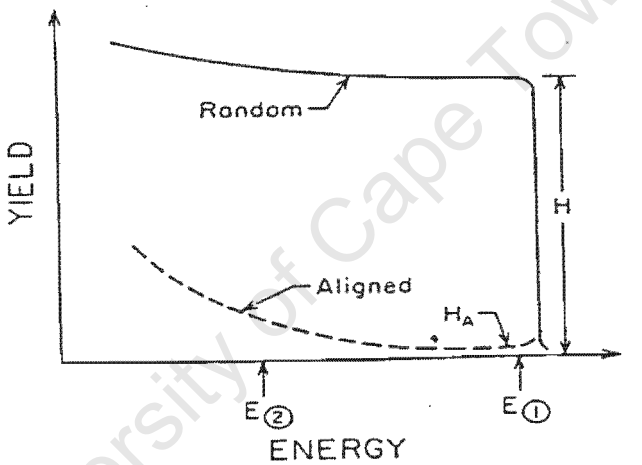

Figure 2-12: *The minimum yield $\chi_{\min}$, which is a measure of the crystalline quality, is defined by the ratio of the aligned yield to the random yield in the near surface regions.*

Chapter 3

Results

3.1 Epitaxially stabilized NiSi silicides

The samples with a 700-Å thick film of nickel on Si<111> substrate were thermally annealed at 450°C to form (equilibrium) nickel monosilicide layers. In the bulk form, and in thin films, NiSi has a orthorhombic MnP crystal structure and cannot grow epitaxially on the cubic silicon substrate and therefore channelling is not observed in silicides thus prepared. These silicides were subsequently laser annealed in the energy density range between $0.5 - 1.0\ J/cm^2$ in an attempt to produce epitaxially stabilized silicides. Some of the silicides were subjected to post-thermal treatment to test the thermal stability of the metastable silicides phases produced by the laser annealing.

3.1.1 NiSi on a <111> substrate

Fig. 3-1 shows the RBS and channelling spectra taken after laser annealing at an energy density of $0.53\ J/cm^2$. Also shown is a random RBS spectrum of as-prepared NiSi taken from outside the laser annealed spot. The presence of channelling in the film is an indication that complete melting of the film has occurred allowing for re-ordering of atoms in the melt and subsequent epitaxial regrowth on the substrate. Epitaxial alignment of the film with the substrate is more pronounced in the interface region. Even though

complete melting in the film was clearly induced by the laser pulse, there is essentially no difference in the random spectra taken from inside and outside the laser spot. This confirms that little or no intermixing between the silicon from the substrate and the NiSi film took place suggesting that no melting of the substrate took place. Other samples were subjected to laser annealing at higher energy densities.

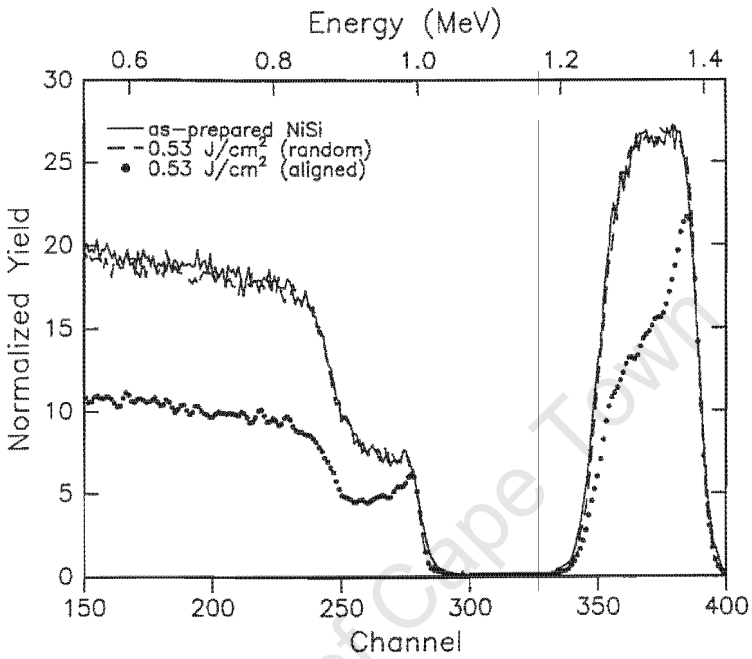

Figure 3-1: *RBS spectra of the as-prepared NiSi sample and after annealing at energy density 0.53 J/cm^2. The similar height and width of the random spectra indicate that the film is still NiSi after the laser anneal.*

RBS and channelling spectra of samples laser annealed in the energy density range $0.5 - 1.0\ J/cm^2$ are shown in fig. 3-2. The rapid decrease in $\chi_{\min}$ as the energy density increases indicates that the epitaxy of NiSi film improved with increased laser energy. Atomic alignment of the NiSi with the substrate begins at the Si/silicide interface with the channeled/nonchannelled interface moving towards the surface of the film as energy density is increased. The channeled/nonchannelled interface almost completely disappears after annealing at energy density 0.92 J/cm^2 resulting in uniformly ordered

film.

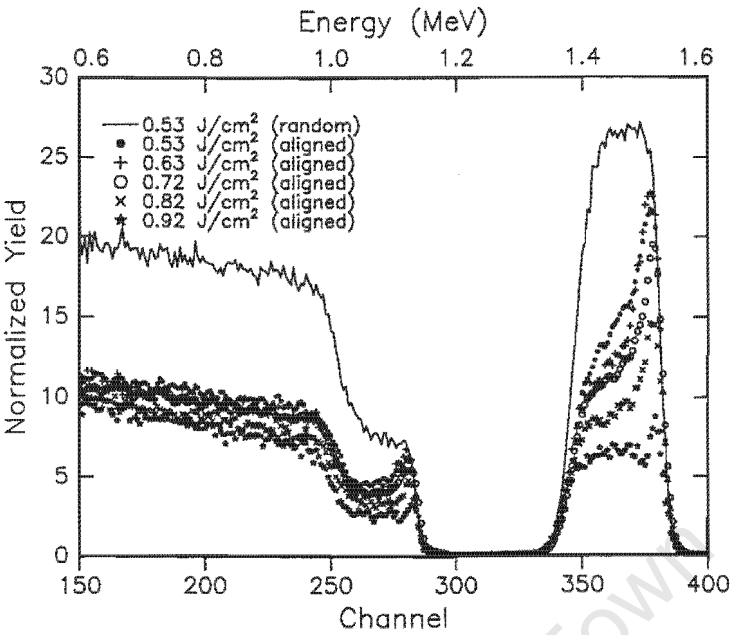

Figure 3-2: *RBS and channeling spectra taken for NiSi samples laser annealed in the energy density range* $0.5 - 1.0\ J/cm^2$. *The decrease in the height of the aligned spectra as the energy density is increased indicates the improvement in the epitaxial quality of the film.*

The best $\chi_{\min}$ for the NiSi film of $\sim 25\%$ was achieved after annealing at $0.92\ J/cm^2$. A significant amount of interdiffusion between the NiSi film and silicon from the substrate was, however, found to have occurred after this laser anneal. The decrease in the height and the broadening of the Ni peak in the random RBS spectra shown in fig. 3-3 indicates that the melt front not only melted the whole of the NiSi film, but it also penetrated through into the substrate. Because of the rapid diffusivity in the melt, diffusion of silicon into the NiSi film takes place. Subsequently the undercooled melt regrows epitaxially on the substrate when the solid-liquid interface moves back to the surface of the sample. The resultant surface layer has a composition ranging from $NiSi_{1.8}$ near the Si/silicide interface to $NiSi_{1.5}$ at the surface.

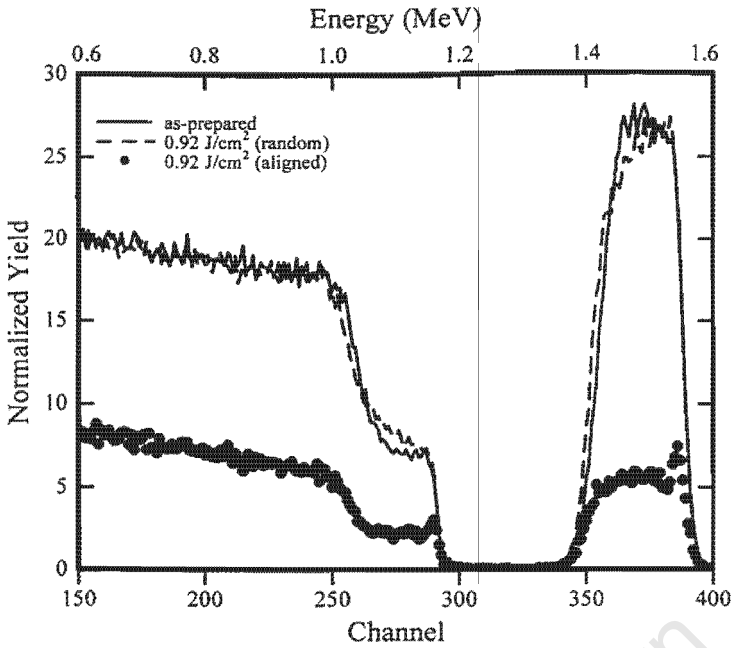

Figure 3-3: *RBS and channeling spectra of the sample annealed at 0.92 J/cm^2 together with the spectrum for the as-prepared NiSi sample. The decrease in height of the random spectra after annealing at 0.92 J/cm^2 shows that the film is no longer stoichiometric.*

3.1.2 Effects of multishots on NiSi

One of the major drawbacks of laser annealing is that it is a non-equilibrium process and can therefore produce silicide layers of continuously varying composition. In an attempt to produce silicide layers with a more uniform composition throughout, the use of multishot laser pulses was also investigated. Fig. 3-4 shows a schematic diagram of a sample subjected to multishots of laser pulses with an energy density sufficient to melt the silicide film and some silicon from the substrate. If the energy density is kept constant, the melt depth should remain unchanged from shot to shot. During the first pulse the whole of the silicide film melts, together with a small portion of the silicon substrate (b). Some silicon diffuses into the silicide film before recrystallisation sets in, resulting in a silicide film with a non-uniform distribution (c). In subsequent shots intermixing will only occur within the melt (i.e. no more silicon will diffuse into the molten region). With

each shot (laser pulse) the silicon in the melt will therefore become more and more evenly distributed, and the silicide layer should end up with a uniform silicon distribution, even though the composition may be non-stoichiometric (e).

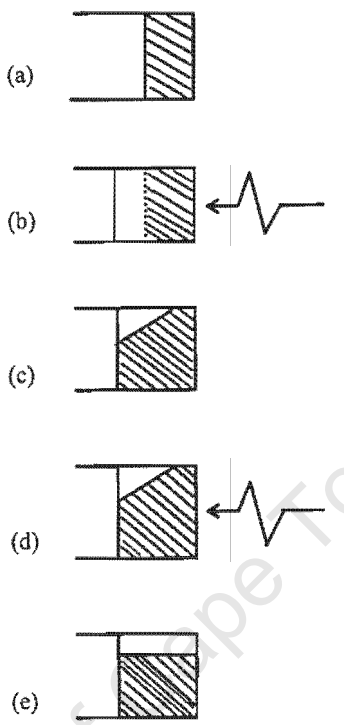

Figure 3-4: *The schematic representation of a silicide film which is laser annealed with series of shots of same energy density.*

In this investigation the NiSi films subjected to up to 8 multiple laser pulses in the energy density range $(0.5 - 0.7\ J/cm^2)$ to study the effects of multishot radiation in the composition of the silicide layer. Fig. 3-5 shows random spectra after laser annealing of samples at laser energy densities $0.54\ J/cm^2$ and $0.69\ J/cm^2$ for different number of shots. Following 2 shots in both cases there was a further drop in height in Ni signal. However this was accompanied by an increase in thickness of the Ni signal, which is contrary to what was expected because this suggests that additional silicon had diffused into the silicide film from the substrate during the laser anneal. This is probably due to

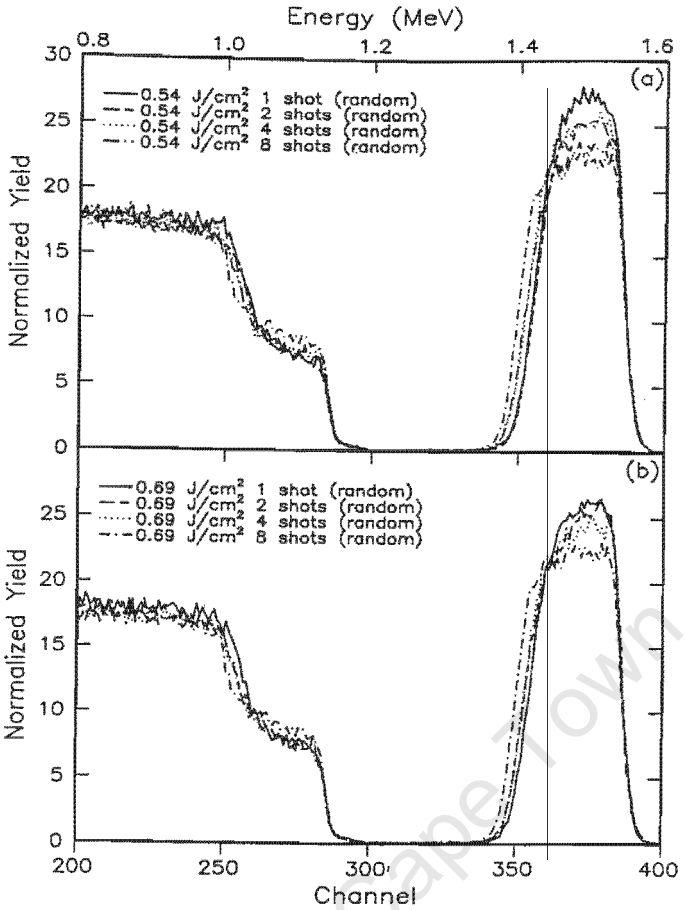

Figure 3-5: *The RBS spectra for samples subjected to 1, 2, 4 and 8 consecutive laser pulses in the energy density in the range* $0.5 - 0.7\ J/cm^2$.

the small variations in the energy of the laser pulse from shot to shot. On the whole, however the general trend is that as the number of pulses increases the composition becomes more uniform throughout the film. This attempt was therefore not a complete success because of the irreproducibility of the laser.

Fig. 3-6 shows a comparison of random and aligned spectra after laser annealing with a single shot at various energy densities. The results for single shot of laser pulses are similar to those obtained earlier as depicted in fig. 3-2. In this investigation the best χ_{min} being achieved was $\sim 50\%$.

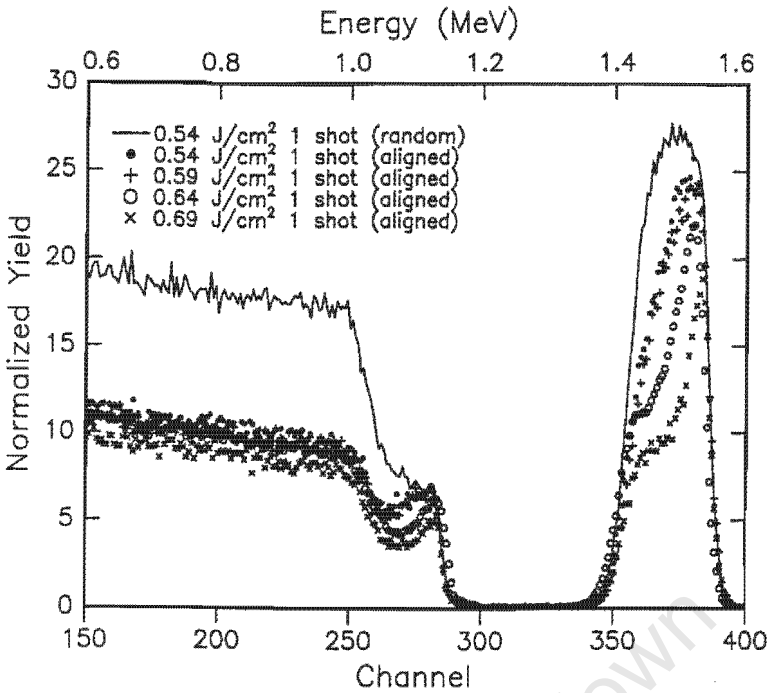

Figure 3-6: *RBS and channeling spectra for NiSi samples laser annealed with single shots of pulses in the energy density range* $0.5 - 0.7\ J/cm^2$.

Fig. 3-7 shows spectra for samples laser annealed at the energy densities 0.54 and 0.69 J/cm^2 (fig. 3-7 (a) and (b) respectively) for 1, 2, 4 and 8 laser pulses (shots). Both sets show that, in general, $\chi_{\min}$ improves with increase in the number of shots, with the $\chi_{\min}$ being lower in the case of higher energy density. With increasing number of shots the channelled/nonchannelled interface also moves towards the surface and in the case of 0.69 J/cm^2 the whole film has become completely aligned with the substrate after 8 shots. One surprising observation found in this investigation was that $\chi_{\min}$ after 2 shots in many cases (but not all) was lower than that following 4 shots. As observed earlier, $\chi_{\min}$ decreases with increase in energy density. Had one of the pulses in the 2 shot sample being significantly higher in energy density than the average, this would explain the $\chi_{\min}$ being lower for 2 shots than for 4 shots. However, were this to occur, the Ni signal in the random spectra following 2 shots should be broader than that following 4

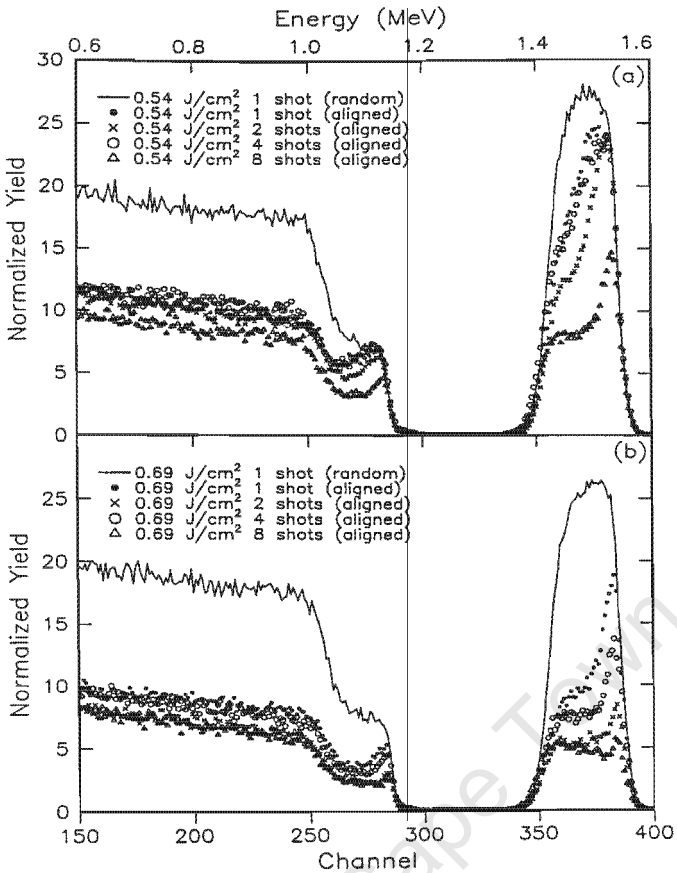

Figure 3-7: *RBS and channeling spectra for samples laser annealed at energy density 0.54 and 0.69 J/cm² with 1,2,4 and 8 consecutive laser pulses.*

shots. Comparison of the random spectra in fig. 3-5 (a) and (b) shows little difference between the two, suggesting that the above explanation is without foundation. It is unclear what the true cause of the behaviour is. Since the lower 2-shots was observed in 80% of the cases it is believed that the effect may well be genuine.

Fig. 3-8 shows a comparison for the random and aligned spectra for 2 and 8 multishots (fig. 3-8(a) and (b) respectively) at energy densities in the range $(0.5 - 0.7\ J/cm^2)$. The results in fig. 3-8 are similar to 1 shot except that $\chi_{\min}$ decreases with an increase in the number of shots, as expected.

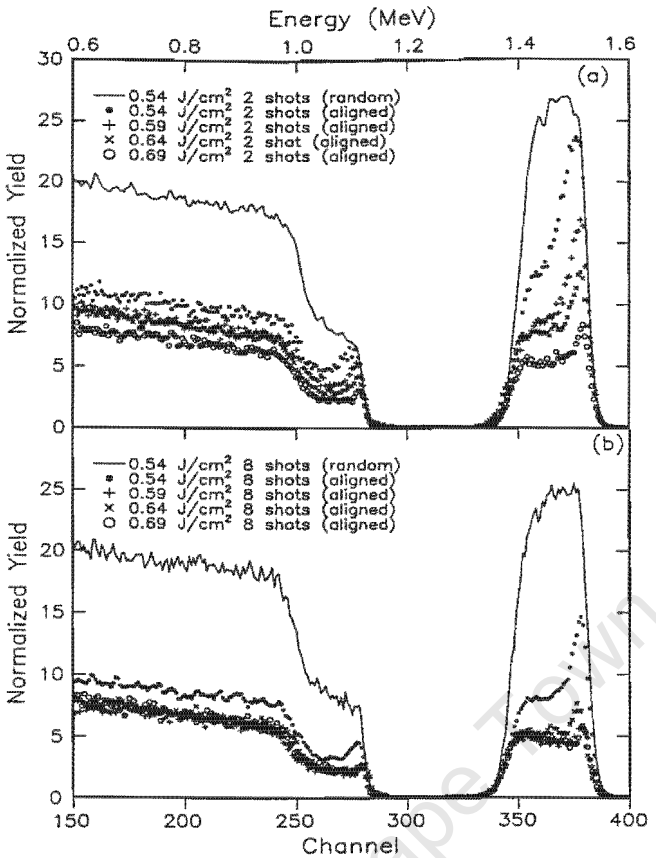

Figure 3-8: *The RBS and channeling spectra for samples subjected to 2 and 8 shots of laser pulses in the energy density range* $0.5 - 0.7\ J/cm^2$ *. Generally the minimum yield decreases with an increase in the energy density.*

3.1.3 Post-thermal treatment of metastable NiSi

The stability of the metastable phase of NiSi produced by the laser anneal was tested by subjecting the films to a thermal anneal at temperatures in the range $150 - 350$°C for 30 minutes. Fig. 3-9 shows the random and aligned spectra from samples laser annealed at energy density of $0.53\ J/cm^2$ and subsequently thermally annealed for 30 minutes at temperatures of 150 and 200°C.

The spectra show that after annealing at 150°C for 30 minutes, channelling in the film detoriated significantly (particularly in the surface region) suggesting that the film in

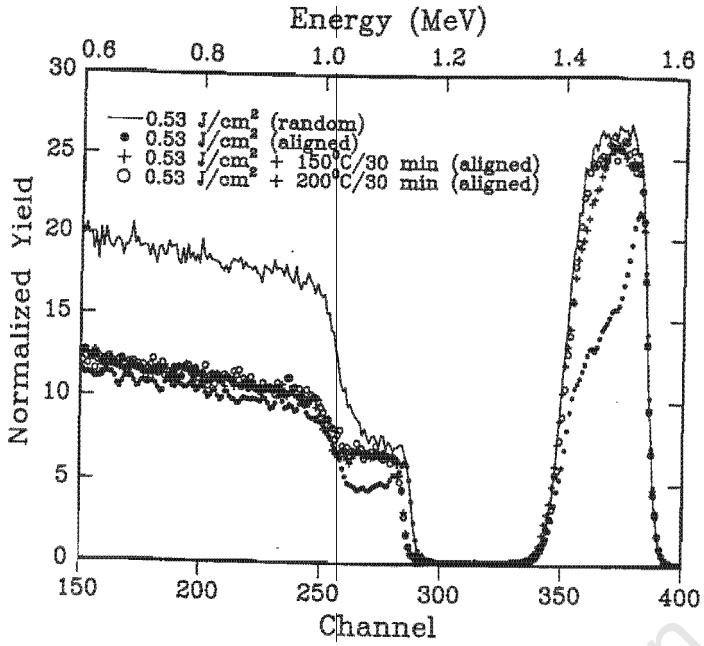

Figure 3-9: *The RBS and channeling spectra to test the stability of the produced metastable phase of NiSi. The samples were subjected to thermal annealing between 150 and 200° C for 30 minutes. Films appear to revert back to the orthorhombic MnP phase of NiSi.*

this region has reverted back to the orthorhombic MnP phase. After the 200°C thermal anneal, the film has almost completely lost any form of channelling which is an indication that the whole film is no longer epitaxially aligned with the substrate.

Fig. 3-10 shows a similar set of spectra from samples laser annealed at a higher energy density 0.92 J/cm^2 and subsequently thermally annealed at temperature in the range 200 – 350°C for 30 minutes. After annealing at 200°C, the aligned spectrum showed a broad increase in the minimum yield in the Ni signal. As the annealing temperature is increased the film loses more and more of its epitaxial quality particularly in the surface region. However the rate at which the epitaxy disappears is much slower than that observed in fig. 3-9. After a 275°C thermal anneal channelling is still observed throughout the film, all be it of poorer quality.

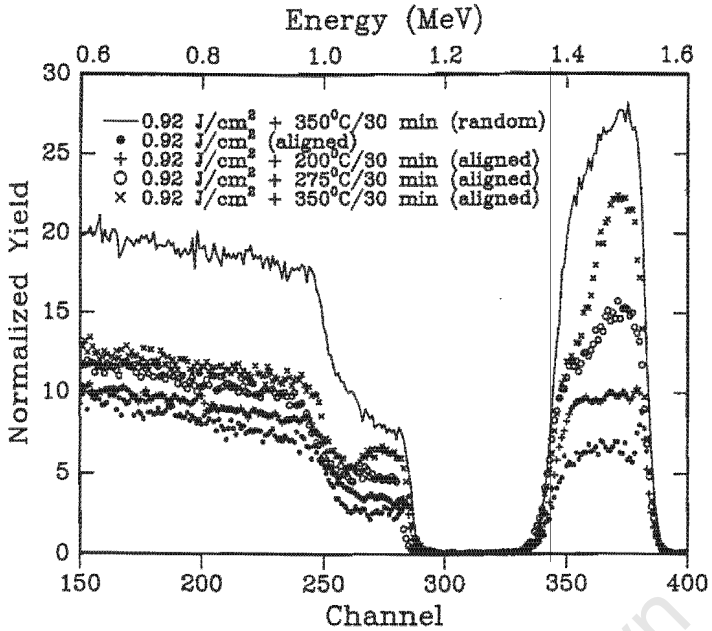

Figure 3-10: *The RBS and channeling spectra for samples subjected to post-thermal anneal in temperatures between 200 and 350° C for 30 minutes. The film slowly looses its epitaxial quality because of too much interdiffusion between NiSi and silicon from the substrate took place*

Even after annealing at 350°C, channelling in the surface region had not completely disappeared indicating that not all of the NiSi in this region had reverted back to the equilibrium phase. Substantial channelling was however still observed in the Si/silicide interface region. This indicates that the metastable phase in the interface region is the most stable. It should be noted that the silicon concentration is significantly higher in this region of the film than in the surface. .

3.2 Epitaxially stabilized CoSi on a <111> substrate

Samples with 500−Å thick films of cobalt on Si<111> were thermally annealed at 450°C for one hour to form (equilibrium) cobalt monosilicide layers. In bulk, and in thin films, CoSi has a cubic ϵ-FeSi crystal structure with a lattice constant of 4.44 Å. Silicon has

cubic diamond crystal structure and lattice constant of 5.43 Å. The mismatch between the two is too large (about 18%) to enable CoSi to grow epitaxially on the silicon substrate and no channelling in thermally produced CoSi is observed.

The thermally produced silicides were subsequently laser annealed in the energy density range between $0.4-0.7\ J/cm^2$ in an attempt to produce epitaxially stabilized silicides. Some of the silicides were subjected to post-thermal treatment to test the stability of the laser induced silicide films.

3.2.1 CoSi on a <111> substrate

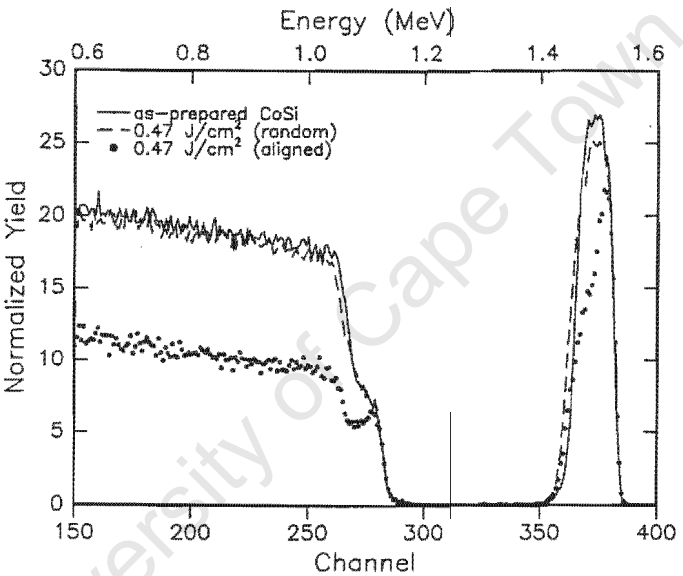

Figure 3-11: *The RBS and channelling spectra for the as-preapred and sample annealed at energy density 0.47 J/cm^2. The height of the as-prepared CoSi and random spectra indicate that the film is longer CoSi, instead a new silicon rich layer has been formed at the Si/CoSi interface.*

Fig. 3-11 shows the RBS and channelling spectra obtained after laser annealing at density of 0.47 J/cm^2. Also shown in the figure is a random RBS spectrum of the as-prepared CoSi (i.e. taken from outside the spot). The appearance of channelling in

the film is an indication that complete melting of the film has occurred, allowing for re-ordering of atoms in the melt and subsequent epitaxial regrowth on the substrate. The epitaxial alignment of the film begins at the Si/silicide interface and is more pronounced in that region.

Comparison of the random spectrum from inside and outside the laser spot shows that the cobalt concentration in the silicide film has decreased and the film has become thicker. This indicates that partial melting of the silicon substrate has occurred, followed by rapid mixing of silicon and silicide in the melt before recrystallization. Consequently, intermixing between the silicon from the substrate and the CoSi film took place, with a silicon rich layer forming at the interface region. Other samples were subjected to laser annealing at higher energies.

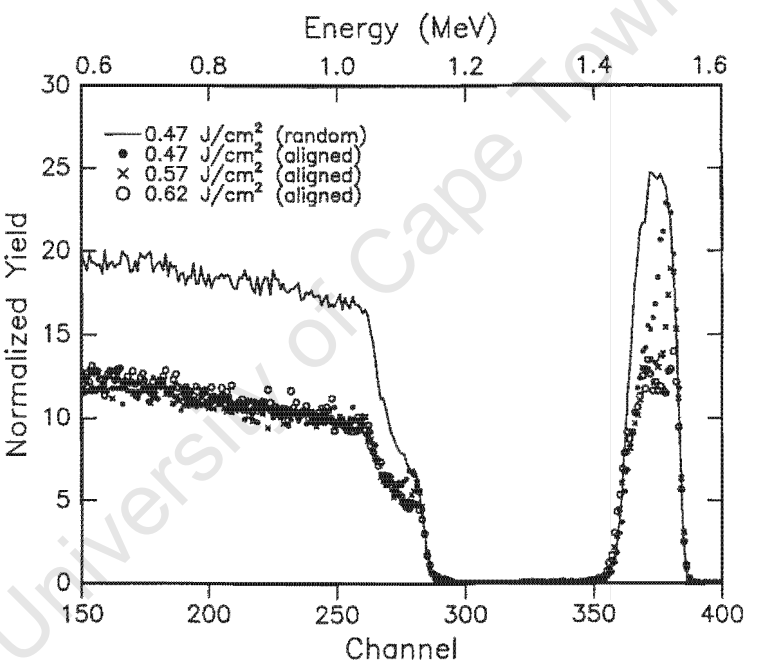

Figure 3-12: *The RBS and channeling spectra for CoSi samples annealed at energy density range* $0.4-0.7$ J/cm^2. *The minimum yield decreases with an increase in energy density.*

Fig. 3-12 shows RBS and channelling spectra for samples laser annealed at energy densities in the range $0.4-0.7\ J/cm^2$. The rapid decrease in $\chi_{\min}$ of the aligned spectra

as the energy is increased indicates that the epitaxy of the CoSi film improved with increased laser energy density. Atomic alignment of the CoSi film with the substrate begins at the Si/silicide interface with the channelled/nonchannelled interface moving towards the surface of the film as energy of laser increase. The best $\chi_{min} \sim 45\%$ was obtained after annealing at energy density 0.62 J/cm^2 as shown in fig. 3-13. However, as the energy density of the laser impulse is increased more intermixing between the silicon substrate and CoSi in the film occurs, particularly in the interface region.

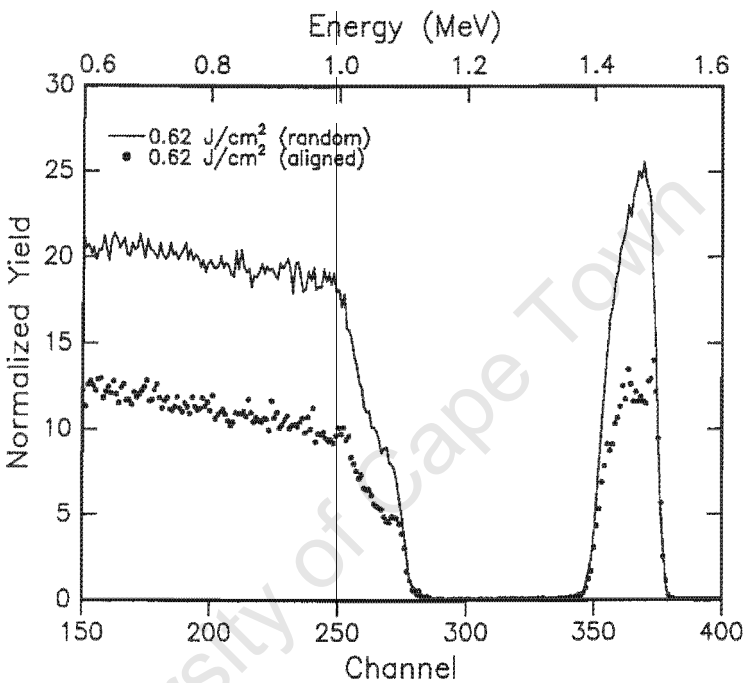

Figure 3-13: *The RBS and channelling spectra showing the best minimum yield of 45% for CoSi samples after annealing at energy density 0.62 J/cm^2.*

3.2.2 Thermal treatment of metastable CoSi

The stability of the metastable phase of CoSi produced by laser annealing was tested by subjecting the films to a thermal anneal at temperatures in the range 200-400°C for one hour. Fig 3-14 shows the random and aligned RBS spectra from samples laser annealed

at energy density 0.52 J/cm^2 and subsequently thermally annealed at 200°C. The spectra shows that channelling in the film had almost completely disappeared, suggesting that most of the film has reverted to the equilibrium ϵ-FeSi phase of CoSi after the thermal anneal.

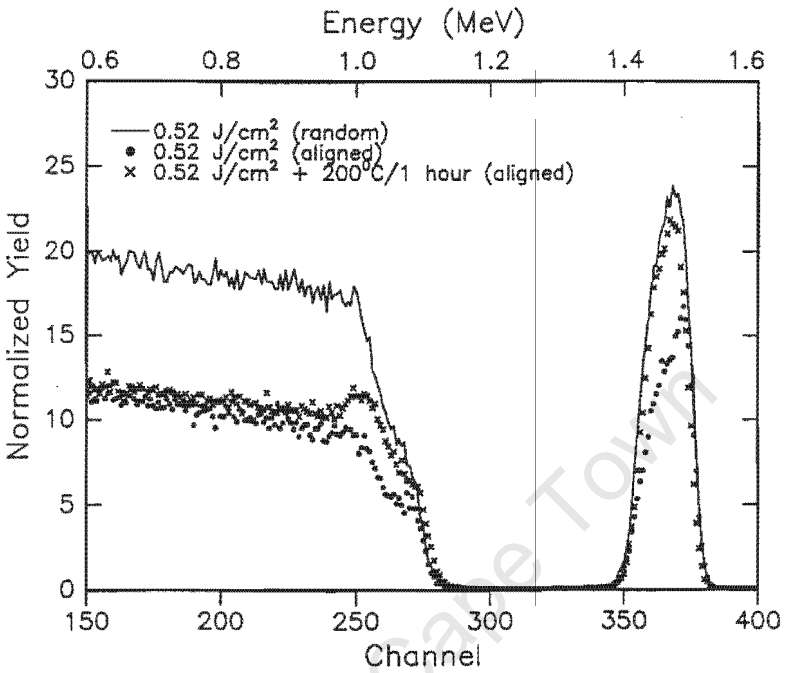

Figure 3-14: *The RBS and channelling spectra for samples annealed at enrgy density 0.52* J/cm^2 *and subsequently thermally annealed at 200°C for one hour.*

Fig. 3-15 shows RBS and channelling spectra from samples laser annealed at higher energy density, 0.65 J/cm^2, and subsequently thermally annealed at temperatures of 250 and 400°C for one hour. After 250°C thermal anneal, there was a notable increase in the χ_{min} of the cobalt signal, particularly in the surface region, suggesting a relaxation of atoms in this region of CoSi layer. As the annealing temperature was increased the film lost more and more of its epitaxial quality particularly in the surface region. However the rate at which epitaxy disappears is much slower than that observed after the lower energy density of 0.52 J/cm^2. The CoSi result are therefore similar in behaviour to those

found with NiSi, i.e. the epitaxially stabilized phase is more stable in the interface region where the silicon concentration is highest. Even after annealing at 400°C, channelling in the interface region had not completely disappeared.

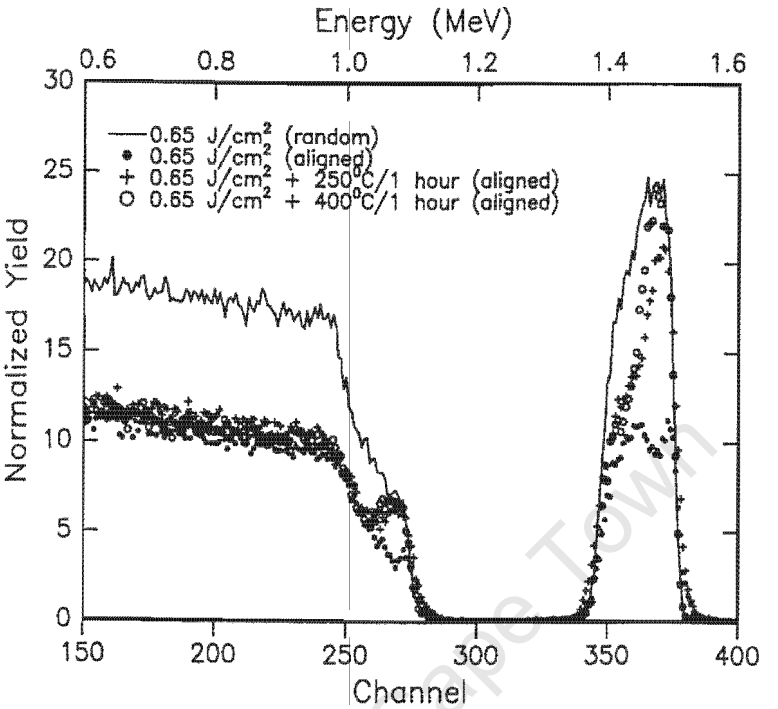

Figure 3-15: *The RBS and channelling spectra to test the stability of the produced metastable phase of CoSi. The samples were laser annealed at 0.65 J/cm² and subsequently thermally annealed at 200 and 450°C for one hour.*

3.3 NiSi/CoSi on a Si<111> substrate

To prevent the problem of interdiffusion between silicon from the substrate and CoSi, a composite NiSi/CoSi film was devised. A Si<111> substrate with 150 Å of nickel and 350 Å of cobalt was thermally annealed at 450°C for 30 minutes in an attempt to form Si<111>/NiSi/CoSi films as discussed in section 2.2.1. These samples were subsequently laser annealed at a energy density in the range $0.3 - 0.7\ J/cm^2$.

Fig. 3-16 shows RBS and channelling spectra taken after laser annealing at low energy densities. Comparison of random and aligned spectra from the sample laser annealed at an energy density of 0.30 J/cm^2 indicate little or no channelling, which suggests that complete melting of the silicide layer did not take place. The presence of channelling in the silicide layer after annealing at an energy density of 0.42 J/cm^2 suggests that the melting had occurred. Channeling in the composite film in the interface region is more uniform, and the boundary between channelled and nonchannelled region is much sharper, than that observed from pure CoSi films (compare fig. 3-12). At first sight this could suggest the presence of an NiSi layer sandwiched between the silicon substrate and the CoSi film as discussed in section 2.2.1. Since NiSi melts at a temperature of 460°C lower than the CoSi, the uniformity at the interface region of the film could be a result of channelling in the NiSi region but not in the CoSi layer. No further change in channelling in the silicide layer was observed up to anneals of energy density 0.62 J/cm^2 and channelling in the surface region was poor. This is contrary to what would have been expected, since for a pure CoSi film an energy density 0.62 J/cm^2 was high enough to produce uniform channelling throughout the silicide film (see fig. 3-12).

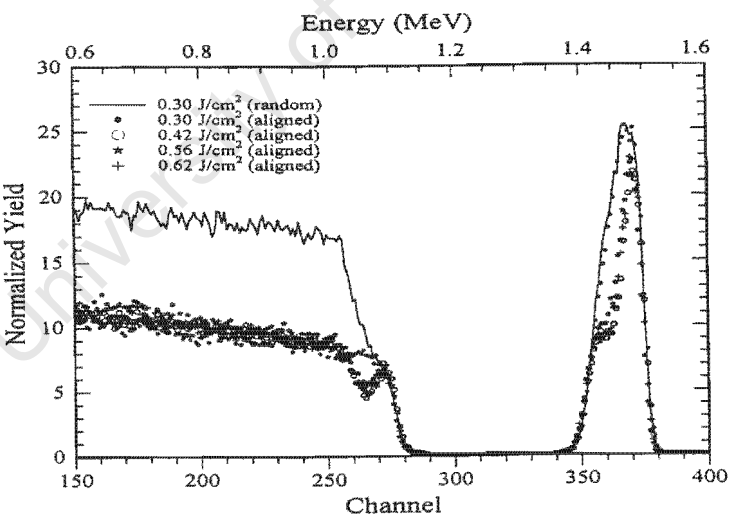

Figure 3-16: *The RBS and channeling spectra for samples with NiSi/CoSi films on the Si<111> substrate annealed at energy density range* $0.3 - 0.7$ J/cm^2.

Fig. 3-17 shows random and aligned RBS spectra for samples subjected to anneals at higher energy densities. The channelling in the film improved slightly after annealing at higher energy density, but χ_{min} is in the surface region remained poor, certainly much worse than in the case of pure CoSi film. The drop in height from the random spectrum indicates that silicon diffusion in the film took place. The poor quality of the films in this particular investigations indicates that it was not possible to eliminate interdiffusion of substrate silicon into the silicide film and the use of composite films in this regard was therefore not a complete success.

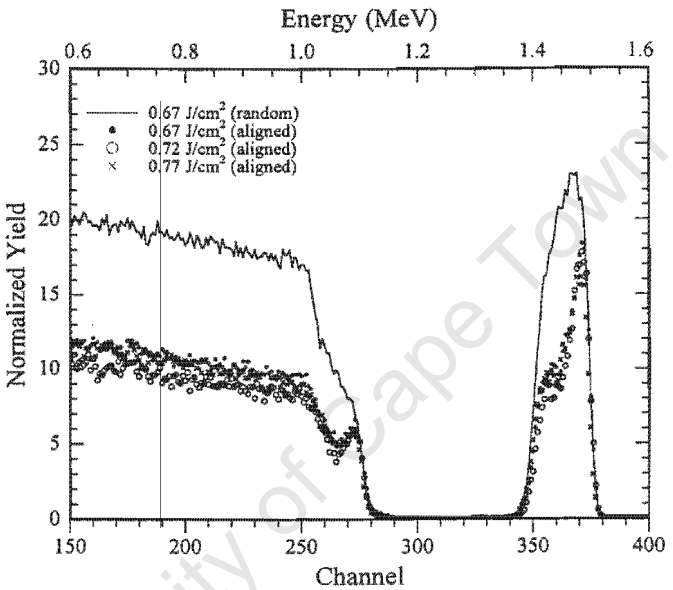

Figure 3-17: *The RBS and channelling spectra for samples annealed in the energy density range* $0.67 - 0.77$ J/cm^2. *A drop in the height of the random spectrum was observed after annealing at energy density 0.67* J/cm^2. *This indicate that interdiffusion has taken place in the Si/silicide interface.*

Chapter 4

Discussion and conclusion

Thermally grown NiSi layers were irradiated with laser pulses in the energy density range between $0.5 - 1.0\ J/cm^2$ in an attempt to produce epitaxially stabilized nickel silicides. The melting of the entire NiSi film without any change in the layer composition occurred after annealing at an energy density $0.53\ J/cm^2$ (see fig. 3-1). Channelling begins in the silicide/Si interface region. As the energy density of the laser pulse was increased the region in which channelling occured broadened. Channelling was observed throughout the film after a $0.92\ J/cm^2$ laser anneal increased. Heat flow computations have shown that an increase in the laser pulse energy density results in a decrease in the solidification velocity of the silicide layer [22]. The solidification of the silicide layer after annealing at energy density of $0.92\ J/cm^2$ will therefore occur at a lower velocity than that after a $0.53\ J/cm^2$ laser anneal. This means that the atoms in the silicide layer have a longer period to re-order after annealing at energy density of $0.92\ J/cm^2$ than after a $0.53\ J/cm^2$ laser anneal. At the higher energy densities of $0.92\ J/cm^2$ (as shown in fig. 3-3) diffusion of silicon from the substrate into the NiSi film resulted in a silicon rich region at the Si/silicide interface. The resultant silicide layer had a composition ranging from $NiSi_{1.8}$ at the interface region to $NiSi_{1.5}$ at the surface of the film. The best χ_{min} achieved was about 25% after a $0.92\ J/cm^2$ laser anneal.

The results observed are similar to those of Baeri *et al.*[22]. Baeri found that the

metastable NiSi phase is cubic and exhibited 3-fold symmetry. It is therefore possible that the cubic phase is the metastable [CsCl]NiSi phase similar to that observed in CoSi and FeSi by von Känel *et al.* Unfortunately it was not possible to identify the phase of the produced metastable NiSi produced by laser irradiation using XRD because the laser spot size was so small that it only represented a small fraction of sample surface (6%). It is interesting to note that von Känel *et al.*[42] have observed the formation of an epitaxial NiSi\NiSi$_2$(type A) from a Si<111>/Ni sample after thermal annealing at 230°C. This silicide was grown by firstly depositing Ni film 18-Å thick on a Si<111> at room temperature followed by a 230°C anneal to form type A NiSi$_2$. Subsequently a 7 Å Ni film was deposited followed by a 230°C anneal to form NiSi.

As mentioned earlier, laser annealing is a nonequilibrium process and usually produces silicide layers of continuously varying composition. The NiSi layers on Si<111> were therefore also subjected to up to 8 multishot laser annealing in the energy density range $(0.5-0.7\ J/cm^2)$ in an attempt to produce non-stoichiometric silicide layers with a more uniform composition throughout. Keeping the energy density constant, the melt depth should remain unchanged. Intermixing should then only occur within the melt during subsequent shots (i.e. no more silicon will diffuse into the molten region). With each shot the silicon in the melt should become more and more evenly distributed, and the silicide layer should therefore end up with a more uniform silicon distribution (even though the composition may be non-stoichiometric). From the random spectra (fig. 3-5 (a) and (b)) for samples annealed at energy densities 0.54 and 0.69 J/cm^2 an increase in the width of the Ni signal was observed as the number of shots increased. This is contrary to what was expected because this indicates that more silicon had diffused into the NiSi layer as number of shots increased. This is probably as a result of slight variations in energy of the laser pulse from shot to shot. However, the composition of the NiSi film did appear more uniform with an increase in the number of shots.

In many cases it was observed (fig. 3-7) that the minimum yield following 2 shots was lower than that for 4 shots. This was originally thought to be due to variations

in energy density of the laser pulse; i.e χ_{min} would be lower for 2 shots than for 4 shots if one of the pulses in the 2 shot sample was significantly higher in the energy density than average. Had this been the case, however, the Ni signal following 2 shots should be broader than that following 4 shots. This was found to be not the case (see fig. 3-5) which suggests that the above explanation does not hold, and that there must be some other cause for the lower χ_{min} following 2-shot. At present there is no explanation for this behaviour. The attempt of producing a NiSi layer with a uniform composition throughout was therefore not a complete success because of the reproducibility in energy of the laser pulse.

The stability of the metastable phase of NiSi produced by single shot was tested by subjecting the metastable phase to furnace annealing. Fig. 3-9 shows spectra from samples laser annealed at a (low) energy density (0.53 J/cm^2) and subsequently thermal annealed at 150 and 200°C for 30 minutes. Much of the channelling in the film had disappeared after the 150°C anneal and the film lost almost any form of channelling after annealing at 200°C for 30 minutes. This suggests that the metastable [CsCl]NiSi phase is relatively unstable and will transform back to the orthorhombic [MnP]NiSi phase following a relatively low temperature thermal anneal.

Fig. 3-10 shows spectra taken from NiSi samples after laser irradiation at a higher energy density of 0.92 J/cm^2 and subsequently thermally annealed for 30 minutes at temperature ranging between 200 and 350°C. After annealing at 200°C, the aligned spectra showed a broad increase in the minimum yield. As the annealing temperature was increased, the film lost more and more of its epitaxial quality, particularly in the near surface region. However the rate at which epitaxy in the film disappeared was much slower than that observed in fig. 3-9, and even after a 350°C anneal substantial channelling was still present in the interface region.

The above results are consistent with those obtained by Pirri *et al.* [30] *and* Hong *et al.* [31] for the metastable $CoSi_{1+x}$. They found that the stability of $CoSi_{1+x}$ depended on the silicon concentration. For $x = 0$ the metastable [CsCl]$CoSi_{1+0}$ is completely transformed

to [ϵ-FeSi]CoSi phase upon annealing at temperatures in the range $350 - 400°C$. For x values in the range $0 < x < 1$ the metastable $CoSi_{1+x}$ evolves into a mixed phase composed of [ϵ-FeSi]CoSi and [CaF_2]$CoSi_2$, upon annealing at 500°C. For x close to 1, $CoSi_{1+x}$ transforms into the more stable CaF_2 upon annealing at $\sim 450°C$. The observed behaviour is not altogether unexpected since NiSi in the MnP phase, and CoSi in the ϵ-FeSi phase, are line compounds and can only exist if the composition is close to 1:1. The same is true for the CaF_2 phase of $NiSi_2$ and $CoSi_2$ where composition has to be close to 1:2. If the composition is between the ratio 1:1 and 1:2 silicon has to diffuse out of the silicide layer till the composition is close to the ratio 1:1 in order to adopt an [MnP]NiSi phase, or silicon has to diffuse into the silicide layer till the composition is close to 1:2 to form the silicon rich [CaF_2]$NiSi_2$ phase.

It should be pointed out that one drawback in using channelling to monitor the thermal stability of the metastable NiSi phase is that channelling would still be present were the phase to transform to [CaF_2]$NiSi_2$. Clearly if channelling disappears, the metastable phase has transformed to [MnP]NiSi since this phase cannot exist in an epitaxial form on Si<111>. However the reverse is not necessarily true i.e. if channelling remains after annealing it could be due to the formation of the epitaxial [CaF_2]$NiSi_2$ phase rather than the continued existence of the metastable phase. The region most likely to convert to the [CaF_2]$NiSi_2$ phase is the interface region since it is the most silicon rich. This could well be the explanation for the continued existence of channelling in this region even after long thermal anneals.

The thermally produced CoSi films on a Si<111> wafers were irradiated with laser pulses in the energy density range $0.4 - 0.7\ J/cm^2$ in an attempt to produce epitaxially stabilized cobalt silicides. Channelling in the film was observed after $0.47\ J/cm^2$ of laser anneal (see fig. 3-11). Epitaxial alignment of the film began at the Si/silicide interface and was more pronounced in that region. Comparison of the random spectra from inside and outside the spot indicated that the cobalt concentration in the silicide film had decreased and the film had become thicker. This indicates that partial melting of

the silicon substrate had occurred, followed by rapid mixing of silicon and silicide, before recrystallization. This resulted in a silicon rich layer being formed at the interface region. Channelling was first observed at the interface region and as the energy density of the laser pulse was increased the channelled region broadened (as shown in fig. 3-12). At the same time more intermixing between the substrate silicon and CoSi layer occurred, particularly in the interface region. The best χ_{min} of about 45% was achieved after annealing at energy density of 0.62 J/cm^2 (see fig 3-13)

Since no channelling is possible in [ϵ-FeSi]CoSi grown on Si<111>, the appearance of epitaxy in the film after the laser anneal is either due to the formation of [CaF_2]$CoSi_2$ or the formation of a metastable silicide phase. Fig. 4-1 shows a comparison of the random and channelling spectra following 0.62 J/cm^2 laser anneal to that from the as-prepared CoSi and a simulated $CoSi_2$ spectrum. The silicide layer obtained is neither of a composition of CoSi nor $CoSi_2$, however the composition is closer to that of CoSi than it is to $CoSi_2$. It is therefore most likely that the silicide phase produced is the metastable [CsCl]$CoSi_{1+x}$ phase, similar to that reported by von Känel *et al.*[29]. It was again not possible to unambiguously identify the phase by XRD because the size of irradiated spot was too small.

The stability of the metastable [CsCl]CoSi phase produced by pulsed laser annealing was tested by subjecting the metastable phase to thermal annealing. Fig. 3-14 shows spectra from CoSi samples laser irradiated at a (low) energy density of 0.52 J/cm^2 and subsequently thermally annealed at a temperature of 200°C for one hour. Channelling in the film detoriated rapidly and had almost completely disappeared after the 200°C thermal anneal, indicating that most of the film had reverted to the equilibrium [ϵ-FeSi]CoSi. This suggests that the metastable [CsCl]CoSi phase produced by the low energy-density anneal is relatively unstable, and readily transforms back to the conventionally [ϵ-FeSi]CoSi phase.

Fig 3-15 shows spectra taken from CoSi after laser annealing at a higher energy density, 0.65 J/cm^2, and subsequently thermally annealed for one hour at 250 and 400°C.

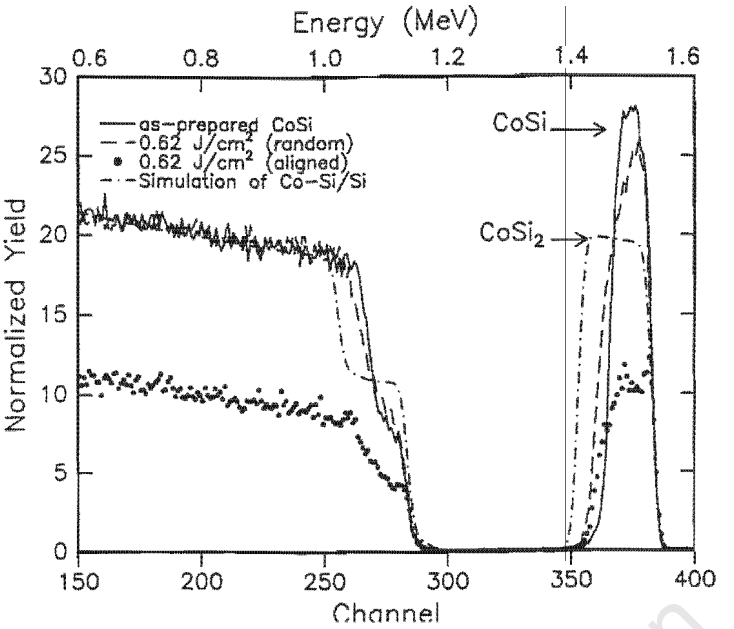

Figure 4-1: *The RBS and channelling spectra taken after subjecting CoSi films to (higher) energy density anneals. Also shown is the spectra for the as prepared sample and $CoSi_2$ simulation.*

After 250°C thermal anneal, there was a notable increase in the χ_{min} of the cobalt signal, particularly in the surface region, suggesting a relaxation of atoms in that region of CoSi layer. As the annealing temperature was increased the film lost more and more of its epitaxial quality, particularly in the surface region. However, the rate at which epitaxy disappeared was again much slower than that observed after the lower energy-density (0.52 J/cm^2) laser anneal, and even after a 400°C anneal, channelling in the inteface region could still be observed. The reason why epitaxy disappeared more slowly in the high energy-density laser annealed sample is probably due to a higher silicon concentration in the silicide film. There is therefore the need for silicon to diffuse out of a region before silicide can convert to the [ϵ-FeSi] phase, or for silicon to diffuse into a region before the silicide convert to the [CaF_2]$CoSi_2$ phase. Since silicon diffusion in silicide at these temperature is expected to be low the process will require a longer period. The reason for the continued epitaxy at the interface is probably due to the

[CsCl]$CoSi_{1+x}$ phase transforming to an epitaxial [CaF_2]$CoSi_2$ phase.

In an attempt to prevent the problem of interdiffusion between silicon and CoSi, a composite NiSi/CoSi film was constructed. A Si<111> substrate with 150 Å of nickel and 350 Å of cobalt was annealed at 450°C in an attempt to form a Si<111>/NiSi/CoSi film as discussed in section 2.2.1. Fig. 3-16 shows spectra taken after laser annealing at an energy densities in the range ($0.3 - 0.6\ J/cm^2$). After $0.30\ J/cm^2$ of laser anneal, little or no channelling occurred which suggested that complete melting of the film had not taken place, while the presence of channelling in the silicide layer after annealing at energy density of $0.42\ J/cm^2$ indicates that complete melting of the film had occurred. No further change in channelling was observed in the silicide layer up to anneals of energy density $0.62\ J/cm^2$.

It was noted that channelling in the interface region was more uniform, and the boundary between the channelled and non-channelled region was sharper, than that observed from a pure CoSi film (see fig. 3-12). Assuming that growth of the composite NiSi/CoSi film on the Si<111> substrate was a success, this would indicate channelling in the buried NiSi layer but not in the surface CoSi layer. With a uniform thin film, laser annealing first causes melting in the surface region of the sample followed by the melt front penetrating deeper in the sample in a uniform manner and the regrowth/recrystallization is also uniform. For composite films melting and recrystallization is not necessarily uniform, i.e. the buried layer could begin to melt before surface layer has completely melted - and the surface layer could begin to solidify before solidification of buried layer had been completed.

Since NiSi melts at a temperature 460°C lower than CoSi, an explanation for the observed behaviour might be that the NiSi layer melted but the whole of the CoSi layer had not melted. Were this to occur, the NiSi layer would have re-crystallized on the single crystal silicon substrate, while the CoSi layer would have re-crystallized on the remaining polycrystalline CoSi film. The NiSi layer would then have regrown epitaxially while the regrown CoSi layer would have been polycrystalline. The above explanation

can not, however, be valid since in the case of a pure 1000-Å thick CoSi film as observed in fig. 3-12 an energy density of 0.47 J/cm^2 was high enough to melt the whole of the 1000-Å thick CoSi layer. These energy densities as shown in fig. 3-16 should therefore be sufficiently high enough to melt the whole of the 690-Å thick CoSi film of the composite film. Clearly the whole silicide layer must have melted after 0.47 J/cm^2 of laser anneal and some other explanation needs to be sought to account for the observed behaviour.

Laser annealing is a non-equilibrium process with the whole laser energy deposited in the surface of the sample, causing melting in the surface region. Heat from the hot region of the sample will then begin to flow deeper into the cooler region of the sample and this can cause further melting. As the heat flows out of the melt its temperature will decrease and when the temperature drops below the melting temperature of the silicide layer, the recrystallization process will begin. With uniform thin films undergoing laser annealing the melt front penetrates into the sample and recedes in a uniform manner. For composite films this need not necessarily be true.

Fig. 4-2 shows a schematic representation of the recrystallization process in a composite NiSi/CoSi film which has been completely melted (assuming that no self diffusion between the NiSi and CoSi layers takes place). Also shown schematically in the figure is the temperature gradient at various times ($t_a < t_b < t_c$). At time t_a, where the temperature gradient is that depicted by curve "a", the whole composite film will be molten. Some time later, time t_b, the temperature gradient will have dropped to curve "b". With this temperature gradient the temperature in the NiSi layer nearest to the silicon substrate will have dropped below the melting temperature of NiSi and thus a NiSi layer of thickness x_b will have re-crystallized on the silicon substrate. The remainder of the NiSi layer and the whole CoSi layer is still molten. At time t_c, the temperature of the melt will have further dropped (curve "c"), and now, although the whole of the NiSi has not re-crystallized, the temperature in a portion of the CoSi layer has dropped below its melting temperature and thus recrystallization in the CoSi layer would have also begun. Thus at time t_c, thickness x_c and x_c' of both the NiSi and CoSi would have re-crystallized

respectively. Should this scenario occur the CoSi film would have begun re-crystallizing on a melt.

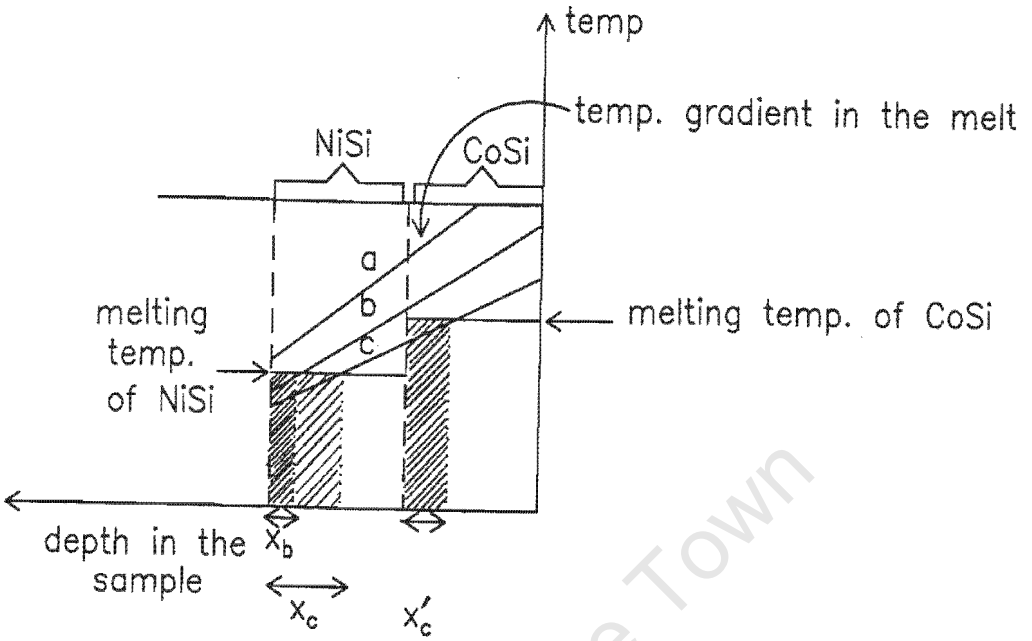

Figure 4-2: *Schematic representation of melting and re-crystallization in a composite film. Symbols a, b and c indicate different temperature gradients in the laser annealed composite NiSi/CoSi film where self diffusion does not take place.*

The above idealized scenario is not possible in real life since self diffusion in the melt is very rapid. Therefore diffusion of nickel from the NiSi region into the CoSi region and cobalt from the CoSi region into the NiSi region would have taken place. Given the rapidity of the laser annealing process the buried layer would, however, still be largely nickel rich while the surface layer would still be largely cobalt rich. Presumably the cobalt rich region would still have a higher melting temperature than the nickel rich region. Were this to occur the NiSi layer would still have re-crystallized on the single crystal silicon substrate, while the CoSi layer would have re-crystallized on a melt. The NiSi layer would then have regrown epitaxially while the regrown CoSi layer would have been polycrystalline. This might explain why it was therefore not possible for the CoSi

layer to regrow epitaxially.

Fig. 3-17 shows a spectra taken after laser annealing at (higher) energy densities in the range $(0.6-0.7\ J/cm^2)$. The spectrum showed a slight improvement of channelling in the film but remained poor in the surface region. The channelled/non-dechannelled interface becomes less sharp. This would be consistent with greater interdiffusion occurring during the extended melt period leading to less pronounced composition difference between the two layers, and smaller difference in melting temperature of two regions. This was accompanied by a drop in height of the random spectrum, indicating that silicon diffusion into the film had taken place.

The above results were not a complete success and the poor quality of the film indicate that it was not possible to grow epitaxially nor to eliminate interdiffusion of silicon from the substrate and the film.

Bibliography

[1] D. M. Wood and A. Zunger; *Phys. Rev. B,* **40,** 4062 (1989).

[2] R. Bruinsma and A. Zangwill; *J. Phys. (Paris),* **47,** 2055 (1986).

[3] W. G. Moffatt; *Handbook of binary phase diagram,* Genium Publishing Corp, New York, (1984), updated as issued.

[4] K. N. Tu, W. K. Chu and J.W. Mayer; *Thin Solid Films,* **25,** 403 (1975).

[5] J. O. Olowolafe, M-A. Nicolet and J. W. Mayer; *Thin Solid Films,* **38,** 143 (1976)

[6] G. J. van Gurp and C. Langereis; *J. Appl. Phys.,* **46,** 4301 (1975).

[7] G. J. van Gurp, W.F. van der Weg and D. Sigurd; *J. Appl. Phys.,* **49,** 4011 (1978).

[8] K. W. Chu, S. S. Lau, J. W. Mayer, H. Muller, and K.N. Tu; *Thin Solid Films,* **25,** 393 (1975).

[9] S. S. Lau and J.W. Mayer; *J. Appl. Phys.7,* **49,** 4005 (July 1978).

[10] D. J. Coe and E. H. Rhodrick; *.J. Phys D,* **9** 965 (1976).

[11] F. M. d' Heurle, C. S. Petersson, J. E. E. Baglin, S. La. Placa and C.Y. Wong; *J. Appl. Phys.,* **55,** 4208 (1984).

[12] P. Villars, L. D. Calvent (Ed's); *Pearson's Handbook of Crystallographic Data for Intermetallic Phases, American Society for Metals, Ohmic,* 1985.

[13] K. N. Tu, E. I. Allessandrini, W. K. Chu, H. Krauutle, and J. W. Mayer; *Jpn. J. Appl. Phys.*, **2**, 669 (1974).

[14] K. N. Tu and J. W. Mayer; in "*Thin Films-Interdiffusion and Reactions*" (J. M. Poate, K.N. Tu and J. W. Mayer; eds.), Wiley, New York, (1978).

[15] C. M. Comrie and J. E. McLeod; *Critical Issues in Semiconductor Materials and Processing Technologies* (Edited by S. Coffa, F. Priolo, E. Rimini and J. M. Poate), 369-376, (1992).

[16] F. M. d' Heurle, C. S. Petersson, L. Stolt, and B. Strizker; *J. Appl. Phys.*, **53,** 5678 (1982).

[17] F. M. d 'Heurle, D. D. Anfiteatro, V. R. Deline, and T. G. Finstad; *Thin Solid Films,* **128,** 107 (1985).

[18] C. A. Crider, J. M. Poate, J. E. Rowe and T. T. Sheng; *J. Appl. Phys.*, **52,** 2860 (1981).

[19] R. T. Tung, J. M. Gibson, and J. M. Poate; *Appl. Phys. Lett.*, **42,** 888 (1983).

[20] R. T. Tung, J. M. Gibson, and J. M. Poate; *Phys. Rev. Lett.*, **50,** 429 (1983).

[21] T. Kawamu, D. Shimoda, and H. Muto; *Appl. Phys. Lett.*, **11,** 101 (1967).

[22] P. Baeri, M. G. Grimaldi, and F. Priolo; *J. Appl. Phys.* 2, **66,** 861 (1989).

[23] J. M. Poate, H. J. Leamy, T. T. Sheng, and G. K. Celler; *Appl. Phys. Lett.*, **33**, 918 (1978).

[24] W. T. Stacy, G. J. van Gurp, G. E. Eggermont, T. Tamminga, and J. R. M. Gijsbers; *Thin Film Interfaces and Interactions,* edited by J. E. E. Baglin and J. M. Poate (Electrochemical Society, Princeton), New Jersey, 442 (1980).

[25] R. T. Tung, J. M. Gibson, and D. C. Jacobson, and J. M. Poate; *Appl. Phys. Lett.*, **43,** 5 (1983).

[26] H. von Känel, K. A. Mäder, E. Müller, N. Onda, and H. Sirringhaus; *Phys. Rev. B (23)*, **45,** 13 807 (1992).

[27] T. B. Massalski (Editor); *Binary Alloy Phase Diagrams (2^{nd} Ed.)*, American Society of Metals, Ohio, (1990).

[28] L. N. Finnie; *J. L. Less-Common Met.* , **4**, 24 (1962).

[29] H. von Känel, C. Schwarz, S. Goncalves-Conto, E. Müller, L. Miglio, F. Tavazza, and G. Malegori; *Phys. Rev. Lett.* 7, **74,** 1163, (1995).

[30] C. Pirri, S. Hong, M.H. Tuilier, P. Wetzel, and G. Gewinner; *Physical Review B*, 3 , **53,** 1368 (1995).

[31] S. Hong, P. Wetzel, G. Gewinner, and C. Pirri; *J. Vac. Sci. Technol. A* 6 , **14,** 3236 (1996).

[32] D. L. Huestis, G. Marowsky and F. K. Tittel; *Topics in Applied Physics, Excimer Lasers,* edited by Ch. K. Rhodes, Springer-Verlag Berlin Heidelberg **40** 181 (1984).

[33] William T. Silfvast; *Laser Fundamentals*, Cambridge University Press (1996).

[34] Orazio Svelto, David C. Hanna; *Principle of Lasers 3^{rd} edition,* (Plenum Press. New York and London) (1989).

[35] A. K. Antonenko, N. N. Gerasimenko, A. V. Dvurechensky, L. S. Smirnov, G. M. Tseitlin; *Sov. Phys.-Semicond. (Engl. Transl.)*, **10**, 81 (1976).

[36] B. R. Schroeder; *Laser induced epitaxy of Ni and Co silicides,* M.Sc. Thesis, (University of Cape Town) (1994).

[37] T. G. Finstad; *Thin Solid Films,* **51,** 471 (1978).

[38] G. Ottaviani, K. N. Tu, W. K. Chu, L. S. Hung and J. W. Mayer; *J. Appl. Phys.*, **53,** 4903 (1982).

[39] Wei-Kan Chu, James W. Mayer, Marc-A. Nicolet; *Backscattering Spectroscopy*, Academic Press (1978).

[40] Leornard C. Feldman, James W. Mayer; *Fundamentals of Surface and Thin Film Analysis*, Elsevier Science Publishing Co. (1986).

[41] Leornard C. Feldman, James W. Mayer, S. Thomas Picraux; *Materials Analysis by Ion channelling*, Academic Press (1982).

[42] H. von Känel, R. Stalder, H. Sirringhaus, N. Onda and J. Henz; *Applied Surface Science,* **53,** 196 (1991).